รายงานวิจัยฉบับสมบูรณ์

การศึกษาการควบคุมการเกิดโปรตอนเนชั่นของสารตัวกลาง C4a-(hydro)-peroxyflavin ในปฏิกิริยาของเอนไซม์ลูซิเฟอเรส

Investigation on the control of protonation status of C4a-(hydro)peroxyflavin in bacterial luciferases with fast and slow light decay kinetics.

โดย ผศ.ดร. รัชนก ตินิกุล

มกราคม 2561

สัญญาเลขที่ TRG5880106

รายงานวิจัยฉบับสมบูรณ์

การศึกษาการควบคุมการเกิดโปรตอนเนชั่นของสารตัวกลาง C4a-(hydro)-peroxyflavin ในปฏิกิริยาของเอนไซม์ลูซิเฟอเรส

Investigation on the control of protonation status of C4a-(hydro)peroxyflavin in bacterial luciferases with fast and slow light decay kinetics.

ผศ.ดร. รัชนก ตินิกุล
มหาวิทยาลัยมหิดล

สนับสนุนโดยสำนักงานกองทุนสนับสนุนการวิจัยและ
มหาวิทยาลัยมหิดล

Abstract

Project Code : TRG5880106

Project Title : Investigation on the control of protonation status of C4a-(hydro) peroxyflavin in bacterial luciferases with fast and slow light decay kinetics.

Investigator : Asst. Prof. Dr. Ruchanok Tinikul

E-mail Address : ruchanok.tin@mahidol.ac.th

Project Period : 2 years

In this research, the study of pH-dependent effect was used to elucidate insight into enzyme mechanisms of two different enzyme systems. For the first enzyme system, bacterial luciferase (Lux), the effects of pH on protonation status of reactive flavin-oxygen adduct called C4a-(hydro)peroxyflavin intermediate was investigated. When the intermediate spectra were monitored in WT enzyme, the intermediate with λ_{max} 385 nm was detected at low pH (pH 6.5) and this was shifted to shorter wavelength (λ_{max} 375 nm) at high pH (pH 10.5). The results suggested that an intermediate with longer λ_{max} (385 nm) may represent the protonated form of C4a-hydroperoxyflavin and shorter λ_{max} (375 nm) may represent deprotonated form of C4a-peroxyflavin. When the same experiment was carried out in His44Ala and His44Asp mutants, only intermediate with λ_{max} 385 nm was observed throughout pH 6.5-10.5. This indicated the crucial function of His44 residue in controlling the intermediate protonation status in Lux reaction. The second system is succinic semialdehyde dehydrogenase from *Acinetobacter baumannii* (*Ab*SSADH) that catalyzes the oxidation of succinic semialdehyde to produce succinic acid and NADPH. The enzyme has two conserved cysteines (Cys289 and Cys291) in active site. Burst kinetics of NADPH production revealed by stopped-flow experiments has suggested that the rate-limiting steps of enzymes reaction is associated with steps that occur after the hydride transfer. The site-directed mutagenesis studies demonstrated that Cys289 is the catalytic cysteine. As the magnitude of burst kinetics represents the amount of NADPH formed during the first, pK_a of the Cys289 was calculated from a plot of the burst magnitude *versus* pH as 7.4±0.2 which is comparable to the pK_a obtained from the pH-rate profile of 7.5±0.1. The Cys289 pK_a was also measured based on the ability of *Ab*SSADH to form NADP-cysteine adduct which can be detected by the increase of absorbance at ~330 nm as 7.9±0.2. Based on three methods of pK_a measurements, the pK_a value of Cys289 is 7.4-7.9, indicating that *Ab*SSADH enhances nucleophilicity of the active site cysteine by lowering its pK_a by 0.6-1 unit.

Keywords : pH dependent study, Enzyme mechanism, Bacterial luciferase, and succinic semialdehyde dehydrogenase

บทคัดย่อ

รหัสโครงการ: TRG5880106

ชื่อโครงการ: การศึกษาการควบคุมการเกิดโปรตอนเนชั่นของสารตัวกลาง C4a-(hydro)-peroxyflavin ในปฏิกิริยาของเอนไซม์ลูซิเฟอเรส

ชื่อนักวิจัย: ผศ.ดร. รัชนก ตินิกุล มหาวิทยาลัยมหิดล

E-mail Address : ruchanok.tin@mahidol.ac.th

ระยะเวลาโครงการ: 2 ปี

ในงานวิจัยนี้ได้ใช้ผลของ pH ต่อปฏิกิริยาเอนไซม์ มาใช้ศึกษากลไลการเกิดปฏิกิริยาของรีดอกซ์เอนไซม์ที่แตกต่างกัน 2 ชนิด โดยเอนไซม์ชนิดแรกที่ศึกษา คือ เอนไซม์ลูซิเฟอเรสจากจากแบคทีเรีย หรือ Lux โดยได้ศึกษาการเกิดสารตัวกลาง C4a-(hydro)peroxyflavin ที่สำคัญของปฏิกิริยา น pH ต่างๆ จากการศึกษาสเปกตรัมของสารตัวกลาง C4a-(hydro)peroxyflavin ที pH ต่างกันพบว่า เมื่อทำปฏิกิริยาที่ pH 6.5 สเปกตรัมของสารตัวกลางมีค่า λ_{max} 385 นาโนเมตร ในขณะที่พบสเปกตรัมของสารตัวกลางที่มีค่า λ_{max} 375 นาโนเมตร ในภาวะที่ pH สูง (pH 10.5) ซึ่งแสดงให้เห็นว่าสารตัวกลาง C4a-(hydro)peroxyflavin มีการเปลี่ยนแปลงโปรโตเนชั่น โดยสารตัวกลางมีค่า λ_{max} 385 นาโนเมตร น่าจะอยู่ในรูป protonated ในขณะสารตัวกลางที่มีค่า λ_{max} 375 นาโนเมตร น่าจะสัมพันธ์กับสารตัวกลางในรูป deprotonated นอกจากนี้งานวิจัยยังพบกรดอะมิโนที่สำคัญ ที่มีบทบาทสำคัญในการควบคุมโปรโตเนชั่นสารตัวกลาง C4a-(hydro)peroxyflavin ซึ่งสำคัญต่อค่า quantum yield หรือแสงที่เปล่งออกมาจากปฏิกิริยาของ Lux ซึ่งได้แก่กรดอะมิโนฮิสติดิน ตำแหน่งที่ 44 การค้นพบนี้ทำให้เราเข้าใจบทบาทของกรดอะมิโนใน active site ของ Lux ที่จะมีประโยชน์ในการปรับปรุงการเปล่งแสงของปฏิกิริยาได้ สำหรับปฏิกิริยาเอนไซม์ที่สอง คือ เอนไซม์ซัคซินิก เซมิเอลดีไฮด์ ดีไฮโดรจีเนส (SSADH) ที่เร่งปฏิกิริยาการเปลี่ยนสารซัคซินิก เซมิเอลดีไฮด์ เป็นกรดซัคซินิก การค้นพบ burst kinetics ในการเกิดผลิตภัณฑ์ NADPH ทำให้ทราบว่า rate limiting step ของปฏิกิริยาเอนไซม์นี้เกี่ยวข้องกับขั้นตอนหลังจากการสร้างผลิตภัณฑ์ NADPH จากการวิเคราะห์บทบาทของกรดอะมิโน Cys289 และ Cys291 ใน active site ของเอนไซม์ SSADH ทำให้ทราบว่ากรดอะมิโน Cys28 มีบทบาทในการเร่งปฏิกิริยา นอกจากนี้ยังได้พัฒนาวิธีใหม่การติดตาม pK_a ของกรดอะมิโน Cys289 โดยใช้ burst kinetics และการเกิด NADP-cysteine adduct ทำให้ทราบค่า pK_a ของกรดอะมิโน Cys289 ในกลุ่มเอนไซม์ SSADH เป็นครั้งแรก ซึ่งมีค่าเท่ากับ 7.4±0.2 ค่าที่ได้แสดงให้เห็นว่า active site ของเอนไซม์ SSADH มีบทบาทสำคัญในการช่วยเพิ่ม nucleophilicity ของกรดอะมิโน Cys289 ทำให้เอนไซม์สามารถทำงานได้อย่างมีประสิทธิภาพมากขึ้น

คำหลัก : การศึกษาผลของ pH กลไกการเกิดปฏิกิริยาเอนไซม์ เอนไซม์ลูซิเฟอเรสจากแบคทีเรีย และ เอนไซม์ซักซินิกดีไฮโดรจีเนส

Output จากโครงการวิจัยที่ได้รับทุนจาก สกว.

1. ผลงานตีพิมพ์ในวารสารวิชาการนานาชาติ

1.1 **Tinikul, R.,** Chenprakhon, P., Maenpuen, S., Chaiyen, P. Biotransformation of Plant-Derived Phenolic Acids. Biotech. J. (2018) ***(IF=3.649) In press***

1.2 Thotsporn, K., **Tinikul, R.,** Maenpuen, S., Phonbuppha, J., Watthaisong, P., Chenprakhon, P., Chaiyen P. (2016) Enzymes in the p-hydroxyphenyl acetate degradation pathway of *Acinetobacter baumannii*. *J Mol Cat B: Enzymatic.* 134, 353–366. ***(IF=2.189, h-index = 77)***

1.3 Maenpuen, S., **Tinikul, R.,** Chenprakhon, P., Chaiyen, P. (2018) Production of valuable phenolic compounds from lignin by biocatalysis: state of the art perspective. *Advanced Biotechnology* (Book Series): (Wiley-VCH Verlag, GmbH & Co.), Vol. 1, 105-123.

2. การนำผลงานวิจัยไปใช้ประโยชน์

-

3. อื่น ๆ (เช่น ผลงานตีพิมพ์ในวารสารวิชาการในประเทศ การเสนอผลงานในที่ประชุมวิชาการ หนังสือ การจดสิทธิบัตร)

3.1 นำเสนอผลงานแบบ oral presentation

pH effect study for exploring enzyme mechanisms-case studies from bacterial luciferase and succinic semialdehyde dehydrogenase, Invited speaker APPA-PST, 2017, Chonburi, Thailand

3.2 การยื่นจดสิทธิบัตรและ PCT

2558	องค์ประกอบเครื่องหมายโปรตีน (Protein Marker)	อนุสิทธิบัตร (1503001543)
2558	องค์ประกอบเครื่องหมายโปรตีนที่ติดสี (Pre-stained Protein Marker)	อนุสิทธิบัตร (1503001542)
2559	Fusion bacterial luciferase gene, reporter vector, and assay kit	Patent Cooperation Treaty, PCT (PCT/TH/2016000051)

Research topic I

Investigation on the control of protonation status of C4a-(hydro)peroxyflavin in bacterial luciferases with fast and slow light decay kinetics

1. Introduction

Bacterial luciferase (Lux) is an enzyme catalyzing light emitting reaction. It generates light with about 16% quantum yield by using oxygen to oxidize the substrates which are reduced flavin and long chain aldehyde and yields oxidized flavin, acid and water (Shimomura O., 2006; Tinikul and Chaiyen, 2014). Lux is very useful for bioreporter applications as light from its reaction is convenient for detection. Lux has been used as biosensor for detecting live bacteria (Shaw et al., 1986; Ulitzur et al., 1997), toxicant in environment and food-born pathogen contamination (Loessner et al., 1996; Smartt et al., 2011). It can be used as a reporter gene to monitor gene expression in bacteria and in eukaryotic cells (Werland-Karlsson et al., 2002; Tinikul et al., 2012). Recently, a lot of effort has been tried to generate Lux as *in vivo* bio-imaging tool (Close et al., 2012).

Lux reaction intermediates and mechanism have been extensively investigated using steady and pre-steady state kinetics. As Lux belongs to flavin-dependent monooxygenase, it reaction mechanism occurs through the reactive flavin-oxygen adduct, C4a-(hydro)peroxyflavin. Protonation status of the C4a-(hydro)peroxyflavin intermediate is crucial for determine if the intermediate will act as electrophile or nucleophile (Palfey and McDonald, 2010; Chenprakhon et al., 2014). In Lux reaction, it is believed that the deprotonated form of the C4a-(hydro)peroxyflavin intermediate is an active form to react with aldehyde presumably *via* a nucleophilic attack to form C4a-peroxyhemiacetal intermediate. Light emitting species, C4a-hydroxyflavin, is then generated from the decomposition of this intermediate. However, in the absence of an aldehyde, the C4a-(hydro)peroxyflavin intermediate decays to yield H_2O_2 and oxidized flavin without generating light (Figure 1). The C4a-(hydro)peroxyflavin is a key intermediate for light production because light can be liberated only after the C4a-(hydro)peroxyflavin reacts with aldehyde.

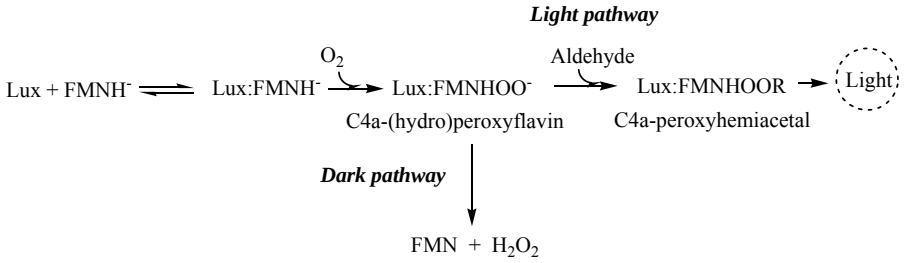

Figure 1 Light and dark pathway of C4a-(hydro)peroxyflavin intermediate in Lux reaction.

Lux can be classified into two types based on light decay kinetics, fast and slow decays (Hosseinkhani et al., 2005). Crucial factors controlling this decay kinetics are currently not known. Studies from our group have previously shown that Lux from *V. campbellii* and *P. leiognathi* TH1 display different kinetics of C4a-(hydro)peroxyflavin formation and H_2O_2 elimination (Tinikul et al., 2013). Different types of Lux may have different controlling mechanism for C4a-(hydro)peroxyflavin formation and this may be relevant to fast and slow light decay kinetics in Luxs. In general, enzymes with slower light decay would give higher signal for luminescence detection and would be more desirable as bioreporters.

Formation of C4a-(hydro)peroxyflavin in flavin-dependent monooxygenases was believed to be initiated by single electron transfer from reduced flavin to dioxygen to generate a redical pair of flavinsemiquinone and superoxide anion. Then, the radical collapses to form the C4a-peroxyflavin adduct which subsequently receives proton to yield a C4a-hydroperoxyflavin (Massey 1994; Chaiyen et al., 2012). Recently, it was discovered that for pyranose-2-oxidase (P2O) and *p*-hydroxyphenylacetate hydroxylase (HPAH), the first step of single electron transfer occurs simultaneously with the proton transfer to form C4a-hydroperoxyflavin (Wongnate et al., 2014; Chenprokhon et al., 2014). These two enzymes have similar features in their active sites in which His is located in proximity to the C4a position of flavin ring and this residue acts as a proton donor at the first electron transfer step.

For Lux reaction, it is conceivable that the deprotonated state of C4a-(hydro)peroxyflavin should be an active form to react with an aldehyde and the control of protonation for C4a-(hydro)peroxyflavin adduct should be different from that of P2O and HPAH. Based on the structure of Lux from *V. harveyi* which is highly homologous to Lux from *V. campbellii,* the only conserved His residue is His44 which is located ~7.5Å from the flavin C4a-position (Campbell et al., 2009) (Figure 2). As it is located too far from the

C4a-position, it is unlikely that it serves as proton donor in the Lux reaction. Therefore, the control of protonation status in lux is still elusive. It is not known if the protonated and deprotonated forms of C4a-(hydro)peroxyflavin can be interchanged at various pH. If it does, what is a pKa associated with this process? How different Lux controls their active site environment to generate C4a-peroxyflavin rather than C4a-hydroperoxyflavin? Our preliminary results of Lux reaction have supported this hypothesis because in the reaction of Lux from *V. campbellii*, showed a different pH-dependent trend on C4a-(hydro)peroxyflavin formation when compared to the reactions of HPAH and P2O.

In this research project, we propose to investigate effects of pH on the steps of C4a-(hydro)peroxyflavin formation and H_2O_2 elimination in Lux reaction using pre-steady state kinetics. The pH-dependent effect will be studied and compared between Lux from *V. campbellii* and *P. leiognathi* TH1 to identify any difference between enzymes having slow and fast light decay kinetics. Site-directed mutagenesis will also be used to investigate the function of the conserved His (His44) that is found in both enzymes from *V. campbellii* and *P. leiognathi* TH1 on the steps of C4a-(hydro)peroxyflavin formation and H_2O_2 elimination. Understanding the mechanism underlying the control of protonation status of C4a-(hydro)peroxyflavin in Lux reaction and if this process is controlled fast and slow light decay enzymes differently should be useful for future enzyme engineering work to improve Lux catalytic efficiency. For example, we may be able to engineer Lux with fast light decay to have slower decay kinetics so that the luminescence is prolonged. This may lead to the improvement of Lux applications because the sensitivity of detection is higher.

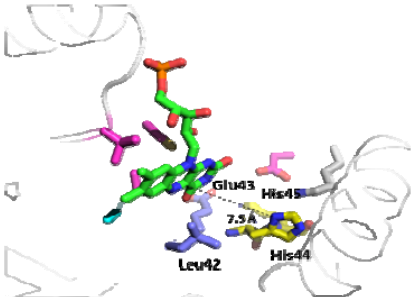

Figure 2 The active site of *V. harveyi* Lux with FMN bound(pdb: 3FGC) reveals 7.5 Å distance of conserve His44 and C4a position of the flavin ring.

2. Objectives

The overall goal of this project is to understand how Lux controls the protonation status of C4a-(hydro)peroxyflavin intermediate. Enzymes with both fast and slow light decay kinetics will be used in this investigation to identify whether their mechanisms in

controlling the intermediate protonation status are different. Pre-steady state kinetics approach will be used as a major technique for this investigation.

Specific aims include:

6.1 To study and compare pH-dependent effects on C4a-(hydro)peroxyflavin formation in Lux from *V. campbellii* and *P. leiognathi* TH1.

6.2 To study and compare pH-dependent effects on H_2O_2 elimination in Lux from *V. campbellii* and *P. leiognathi* TH1.

6.3 To investigate the involvement of the conserved His residue in C4a-(hydro)peroxyflavin intermediate formation in Lux from *V. campbellii* and *P. leiognathi* TH1.

3. Materials and Methods

3.1 Large scale overexpression and purification His44 mutant of Lux_Vc

Lux from *Vibrio campbellii* was overexpressed in 4-L culture. The enzymes were then purified according to methods described in Suadee et al. (2007) and Nijvipakul et al. (2008).

3.2 Effect of pH on fusion luciferase activity

The effect of pH on luciferase activity was investigated by measuring the enzyme activity at various pH values and at 25 °C. Sodium acetate buffer was used for maintaining pH 5.5, sodium phosphate buffer for pH 6.0–8.5, Tris–H_2SO_4 buffer for pH 8.5 and glycine–NaOH for pH 9–10. All buffers were used at a concentration of 50 mM. A bell-shaped profile was obtained by plotting total emitted photons as a function of pH.

3.3 Study of pH-dependent effects on C4a-(hydro)peroxyflavin formation reactions by pre-steady state kinetics

In this experiment, the reaction of Lux:$FMNH^-$ and oxygen in the absence of aldehyde at various pHs was investigated. All reactions was performed at 4^oC using a stopped-flow spectrophotometer in single mixing mode with a one cm optical path length of the observation cell.

3.3.1 pH-jump experiments

In this experiment, the pH of the reaction was rapidly changed upon stopped-flow mixing to test whether the group in the active site that is involved in the protonation of C4a-(hydro)peroxyflavin intermediate can be quickly equilibrated with outside solvent.

FMN (32 μM) and Lux (160 μM from *V. campbellii*) in 10 mM sodium phosphate buffer pH 7.0 was first reduced stoichiometrically in anaerobic glove box with aliquots of ~10 mM sodium dithionite (in 100 mM potassium phosphate, pH 8.0). Reduction of FMN was monitored by a UV-visible spectrophotometer inside a glove box (Belle Technology). The resulting $FMNH^-$ was transferred into a glass tonometer before being loaded onto the stopped-flow machine. The anaerobic solution containing Lux:$FMNH^-$ in the first syringe was mixed with an oxygen (air saturated concentration, 0.26 mM) in various pHs buffers (100 mM sodium phosphate buffer pH 6.0-7.0, 100 mM Tris-HCl buffer pH 7.5-8.5 and 100 mM Glycine-NaOH pH 9.0-10.5)

The reactions was monitored by single wavelength photomultiplier detection at 380 and 450 nm. Observed rate constants of C4a-(hydro)peroxyflavin intermediate formation and H_2O_2 elimination at various pHs was calculated from the absorbance change at 380 and 450 nm. A pK_a value that is associated with the conversion between protonated and deprotonated forms of C4a-(hydro)peroxyflavin was determined by correlating the characteristics of C4a(hydro)peroxyflavin and C4a-peroxyfalvin as a function of pH. The spectra of intermediate at various pH values were determined by diod array mode attached in double mixing stopped flow spectrophotometer.

3.3.2 pH pre-equilibration experiments

FMN (32 μM) and 160 μM Lux from *V. campbellii* in 50 mM buffer at various pH values (6.0, 7.0, 7.5, 8.0, 8.5, 9, 9.5, 10.0, and 10.5) was first reduced stoichiometrically in anaerobic glove box as decribed previously. The resulting $FMNH^-$ was transferred into a glass tonometer before being loaded onto the stopped-flow machine. The anaerobic solution containing Lux:$FMNH^-$ in the first syringe was mixed with the same buffer containing an oxygen (air saturated concentration, 0.26 mM) from the other syringe of the stopped-flow spectrophotometer. The reactions was monitored by photomultiplier detection at 380 and 450 nm. The observed rate constant of C4a-(hydro)peroxyflavin intermediate formation and H_2O_2 elimination obtained from this study will be compared with the data in experiment 3.2.1

3.3.3 pH-Jump experiment carried out in double mixing of stopped flow spectrophotometer

FMN (64 μM) and 320 μM Lux from *V. campbellii* in 50 mM buffer at pH 7.0 was first reduced stoichiometrically in anaerobic glove box as decribed previously.

The anaerobic solution containing Lux:$FMNH^-$ was first mixed with the air-saturated buffer of 100 mM glycine-NaOH buffer pH 10.5. The final pH was brought to 9.8 in the first mix and incubated for 0.2 sec. Then, air-saturated 200 mM sodium phosphate buffer pH 6.5 was added in the second mixing step to give a final pH of 6.9. The spectra of intermediate were monitored by diod array apparatus.

4. Results

4.1 Effect of pH on light emission from Lux reaction

Lux activity was assayed at various pH values to study the effect of pH on light emission. The light emitting profiles was found as bell-shape, the amount of light emitted from Lux reaction increased upon pH increasing and showed optimum pH at around 7. However, when activity was assayed in H44A mutant, there was no light detected in the mutant.

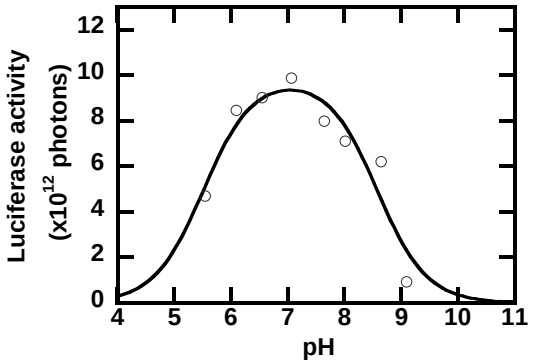

Figure 1 The Lux activity assays were performed at various pHs (pH 5.5-9.0) using a rapid-mixing apparatus and spectrofluorometer at 25°C. The Lux activity at each pH was obtained by integrating the peak area beneath kinetics traces of light emission. The peak area was converted to the total photon emission. The optimum pH of fusion luciferase is 7.0.

4.2 Effect of pH on a reaction of Lux:$FMNH^-$ with oxygen of WT enzyme

The kinetics traces of C4a-(hydro)peroxyflavin intermediate formation of Lux reactions were monitored at absorbance 380 with pH-jump and pre-equilibration experiments.

4.2.1 pH-jump

After an anaerobic solution containing 32 μM $FMNH^-$ and 160 μM Lux_Vc was mixed with buffer containing 0.26 mM O_2 at various pH values. There were three phases of

C4a-(hydro)peroxyflavin intermediate formation in all tested pH values **(Figure 2A)**. However, they showed the difference in intermediate extinction coefficient and behavior. At low pH (pH 6-7.5), the first phase (dead time to 0.02 s) showed rapidly increase of absorbance 380 nm. The second phase (0.02-0.2 s) and third phase (0.2-10 s) showed a small absorbance increase and decrease, respectively. While at higher pH 8.0-9.5, the first phase was the rapid increasing of absorbance 380 nm as found in low pH, but exhibited higher in 380 nm absorption. The second and third phases were a slightly decrease phase of absorbance 380 nm. Observed rate constant (k_{obs}) of absorbance change all phases trended to be pH independent (**Figure 2B**). When the same reaction was monitored at 450 nm, there was no significant change in absorbance even up to 100 s, indicating that there is no oxidation of $FMNH^{\cdot}$ during this period. Plot of absorbance 380 nm change of the first phase versus pH resulted in monosigmodal pH dependent curve and associated with pK_a of 8.3±0.2 **(Figure 2C)**.

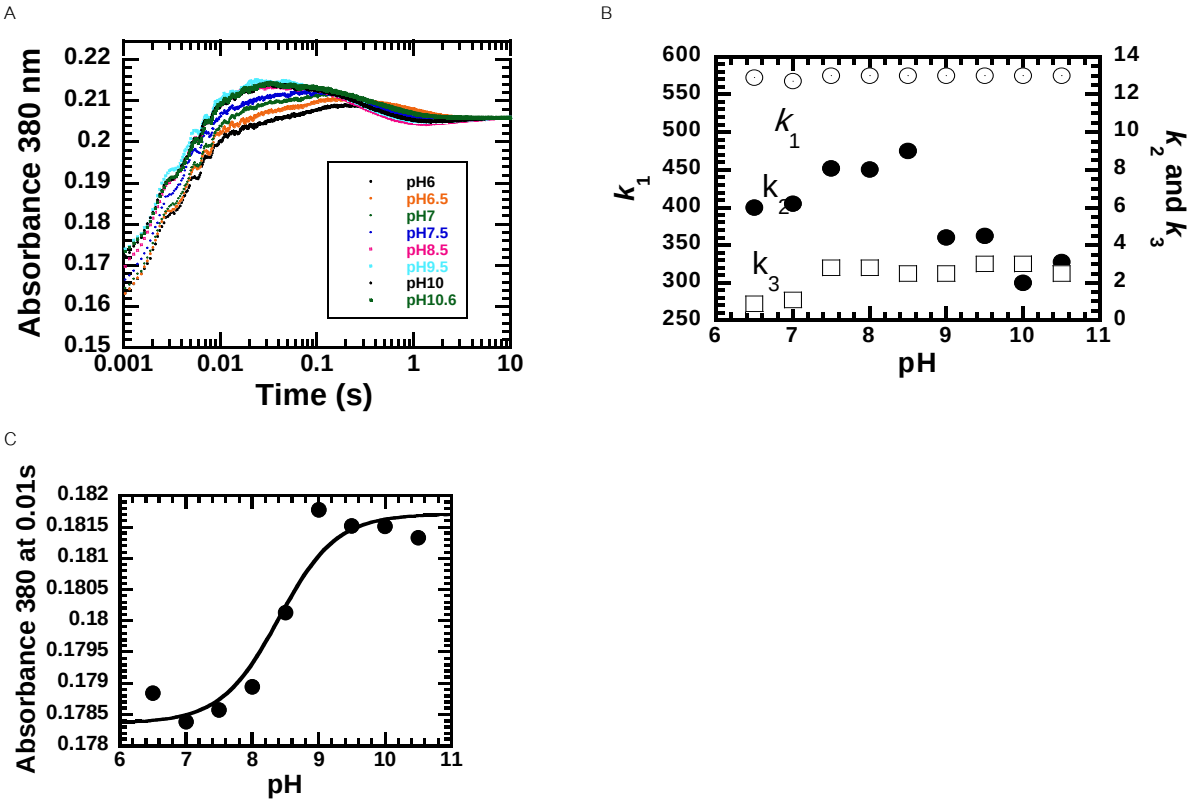

Figure 2 Lux:$FMNH^{\cdot}$ and oxygen reaction at various pH values of WT. Solutions of 80 μM Lux and 16 μM $FMNH^{\cdot}$ in 10 mM sodium phosphate buffer pH 7.0 was mixed with the oxygen (0.26 mM) in buffer at various pH values at 4°C. Concentrations are given as final concentrations after mixing. (A) The kinetic traces of absorbance 380 nm WT (B) A plot of observed rate constants of WT at different pHs. (C) A plot of absorbance 380 nm of the first phase of A versus pHs.

When the reaction of Lux:$FMNH^-$ and oxygen at pH 7 was perform with different oxygen concentrations to see which phase is oxygen dependent. The result showed that only the observed rate constant of the first phase of an intermediate formation was dependent on oxygen concentration (**Figure 3**). This suggests that absorbance increasing at the first phase is the Lux:$FMNH^-$ and oxygen reaction, while the later phases observed in reaction may related to alteration of an intermediate extinction coefficient.

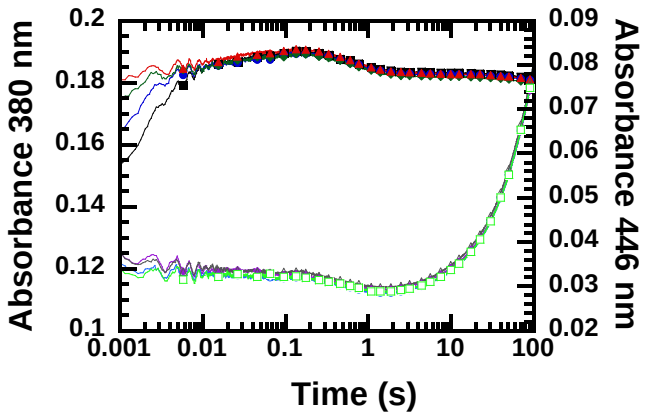

Figure 3 Lux:$FMNH^-$ and oxygen reaction of WT at different oxygen concentrations. An anaerobic solution of 80 μM Lux and 16 μM $FMNH^-$ in 10 mM sodium phosphate buffer pH 7.0 was mixed with the same buffer containing oxygen at 0.13, 0.3, 0.61 or 1.03 mM (from lower to upper traces) at 4°C. Concentrations are given as final concentrations after mixing. The formation of C4a-(hydro)peroxyflavin and flavin reoxidation reaction was monitored at absorbance 380 and 446 nm, respectively.

2.2.2 Intermediate spectra determination

The C4a-(hydro)peroxyflavin intermediate spectra were determined by diod array apparatus attached in stopped flow spectrophotometer. The reactions were performed as described in 2.2.1. The intermediate spectra at 0.005 sec of various pH values were compared. As shown in **Figure 4** , at pH 6.5, the intermediate with a λmax of 385 nm were observed and the λmax of the intermediate was shifted to shorter wavelength (370 nm) when reaction pH was increased. The intermediate with a λmax of 370 nm were observed at pH 10.5. The intermediates are likely to be the flavin C4a-peroxide and C4a-hydroperoxide forms of the enzyme. It was expected that the intermediate with longer λmax found at low pH reaction may associated with the protonated form, C4a-hydroperoxide and the intermediate with shorter λmax found at high pH reaction may associated with the deprotonated form of the flavin C4a-peroxide.

The changing of intermediate spectra upon changing pH values was used to determine pK_a of intermediates and found to associate with pK_a of 8.0±0.4. This value is also consistent with pK_a value calculated from the amplitude change of the first phase of absorbance 380 nm in experiment 3.2.1.

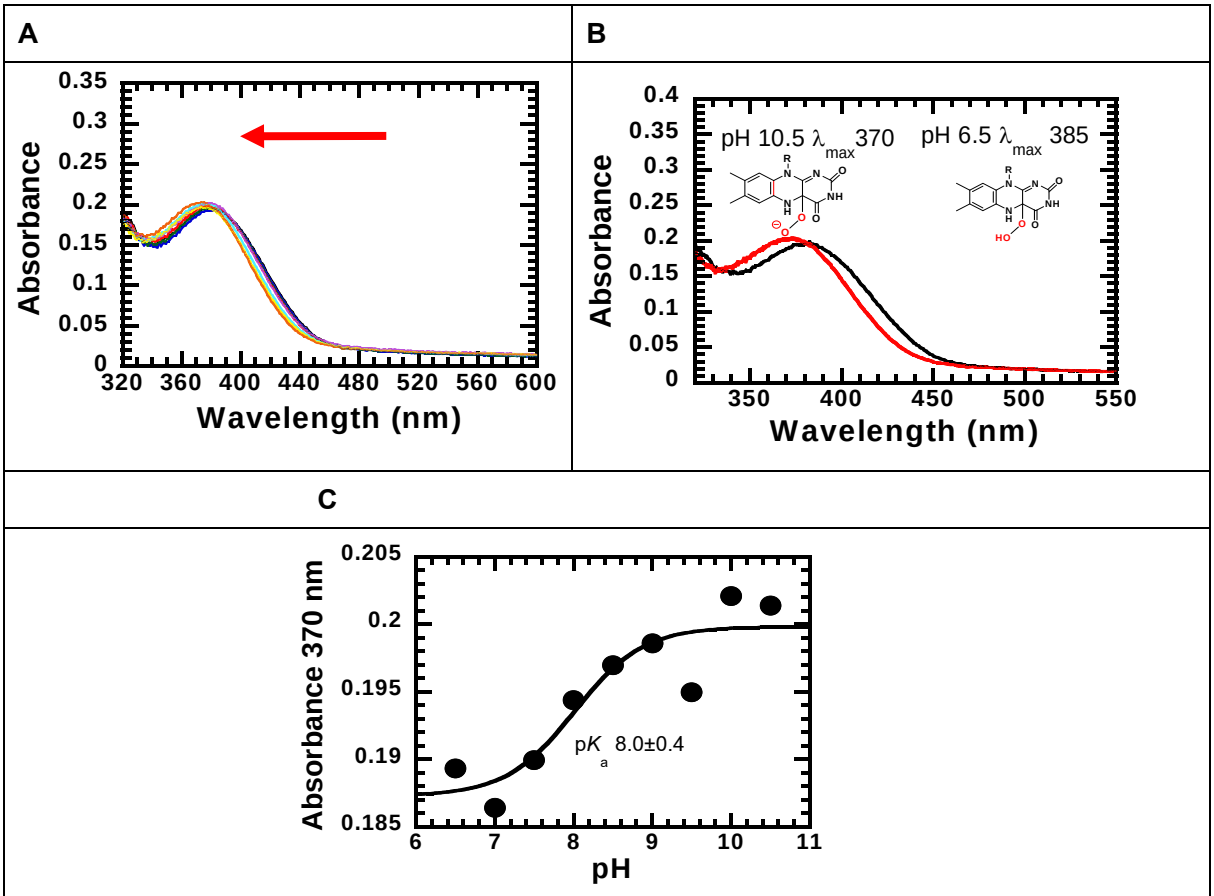

Figure 4 Spectra of the C4a(hydro)peroxyflavin of WT at various pH values**.** Solutions of 80 μM Lux and 16 μM $FMNH^-$ in 10 mM sodium phosphate buffer pH 7.0 was mixed with the oxygen (0.26 mM) in buffer at various pH values at 4°C. (A and B) Intermediate spectra were detected by diod array mode attached with stopped-flow spectrophotometer. (C) Plots of absorbance change *versus* pH values and associated with pK_a of 8.0±0.4.

2.2.3 Pre-equilibration experiments

In pre-equilibration experiments, solutions of Lux_Vc:$FMNH^-$ pre-equilibrated in buffers at different pH values were mixed with the same buffers containing oxygen (0.26 mM) at 4°C. The reactions of C4a-(hydro)peroxyflavin intermediate formation were monitored at low (pH 6.5) and high pHs (pH 9.5). The results showed that at pH 6.5-8, the trend of C4a-(hydro)peroxyflavin formation was similar to the pH-jump experiment with four phases of absorbance 380 nm increasing (**Figure 5A and B**). While at higher pH (pH 9-9.5), there were two phases of absorbance 380 nm. The first phase is C4a-(hydro)peroxyflavin formation because no increasing of absorbance 446 nm was observed at this period. While the second phase was concomitant with the increasing of FMN reoxidation reflected by the increasing of absorbance at 446 nm (**Figure 5C and D**). This is the result of denatured enzyme during pre-incubated at higher pHs. However, at least, the result form pH 6.5-8 can revealed the same in C4a-(hydro)peroxyflavin formation behaviors between the reaction performed by pH-jump and enzyme pre-equilibrated at the same pH C4a-(hydro)peroxyflavin formatio values may imply the fast proton equilibration of the key control group involved in the C4a-(hydro)peroxyflavin formation at the Lux active site.

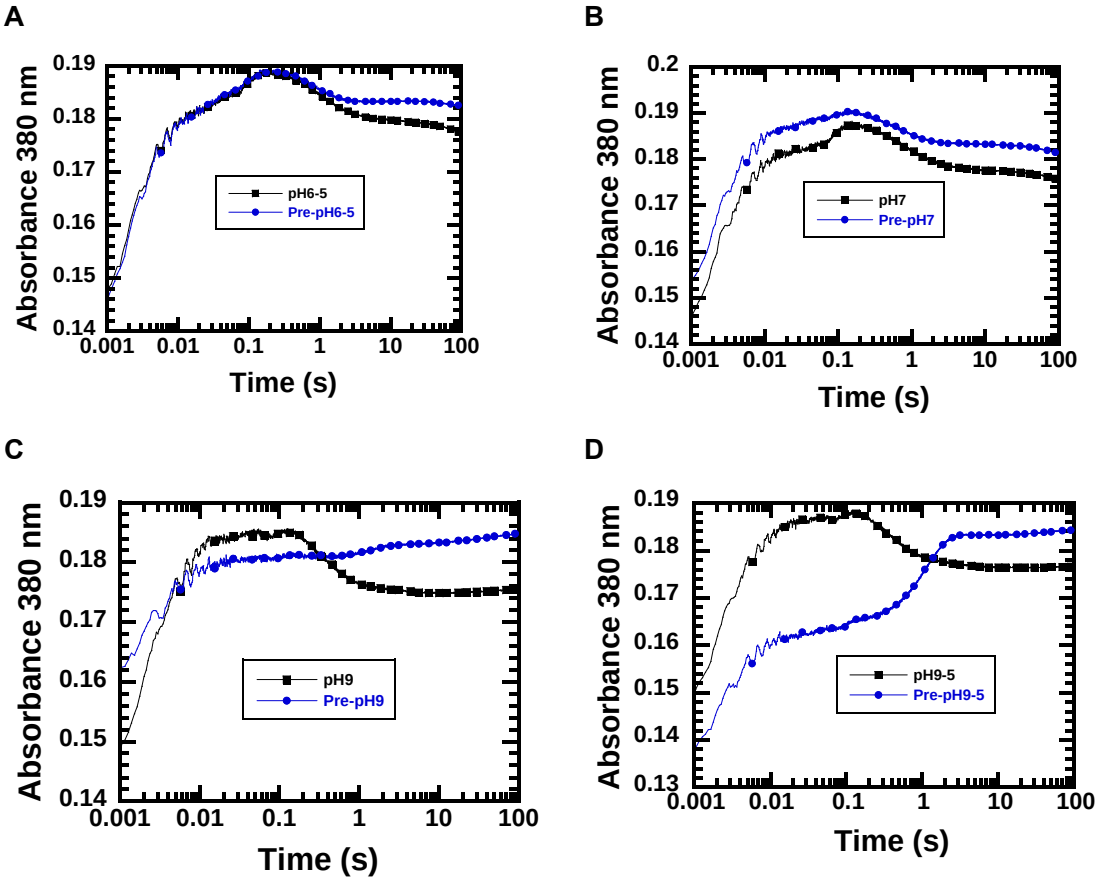

Figure 5 Comparison of C4a-(hydro)peroxyflavin formation traces between pH-jump and pre-equilibrated experiments at various pH values.

2.2.4 Effect of pH on H_2O_2 elimination

For study of pH effect of on H_2O_2 elimination, reactions were performed as described in 2.21. and FMN reoxidation reactions were determined by monitoring at absorbance 446 nm. As shown in **Figure 6A**, the rate of H_2O_2 elimination was found to decrease upon reaction pH was increased from pH 6.5-9. However, when reaction pH was increased higher than pH 9, the H_2O_2 elimination trends to increase **Figure 6B**, which is the result of instability of enzyme in basic pHs. The reduced FMN is liberated from denatured enzyme to be free form and promptly reoxidized to FMN when oxygen comes. The plotted of observed rate constant of H_2O_2 elimination versus pH was shown in **Figure 6C**.

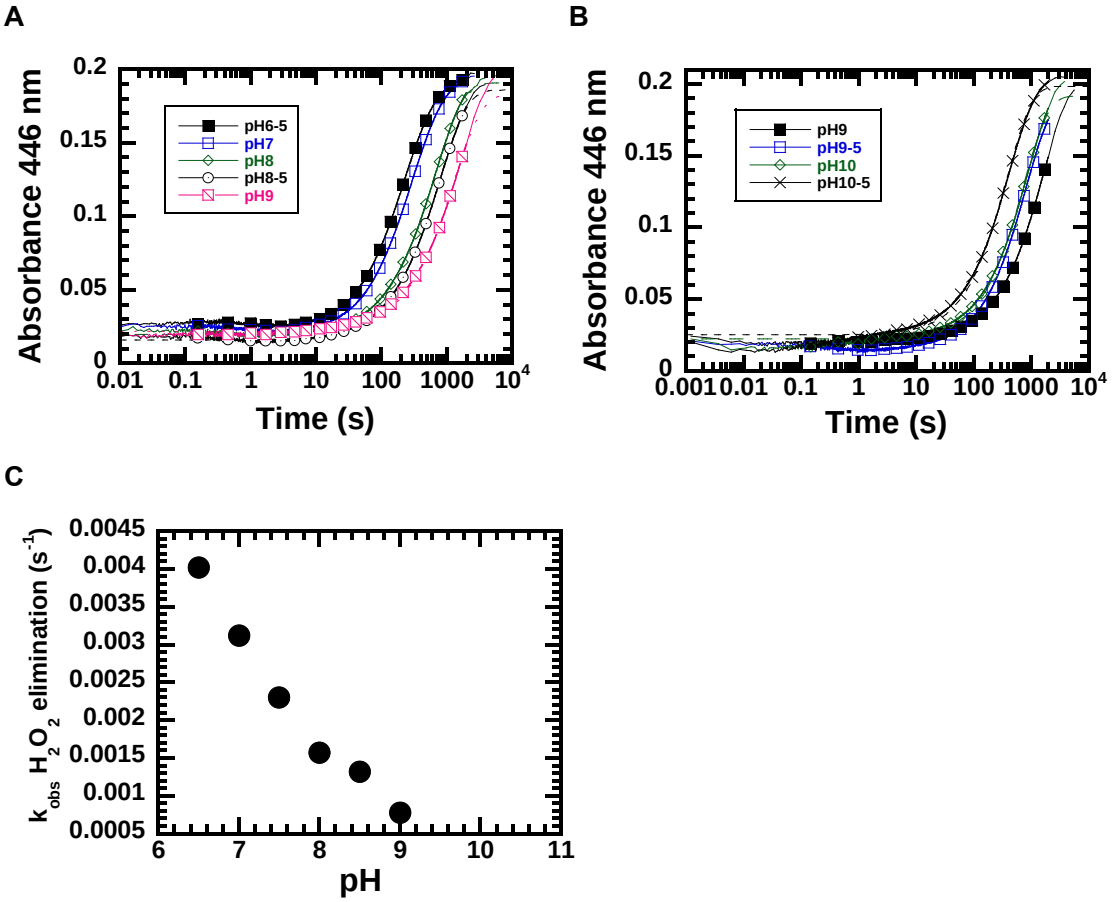

Figure 6 Effect of pH on H_2O_2 elimination in WT enzyme (A and B). Solutions of 80 μM Lux_Vc and 16 μM $FMNH^-$ in 10 mM sodium phosphate buffer pH 7.0 was mixed with the oxygen (0.26 mM) in buffer at various pH values at 4°C and H_2O_2 elimination reaction was monitored at absorbance 446 nm. (C) k_{obs} of H_2O_2 elimination was plotted as function of pH.

2.2 Effect of pH on oxygen reaction of Lux:$FMNH^-$ and H_2O_2 elimination of H44A mutant

The kinetics traces of C4a-(hydro)peroxyflavin intermediate formation and H_2O_2 elimination of H44A mutant were monitored as described in WT enzyme 2.2.1. The C4a-(hydro)peroxyflavin intermediate formation traces in H44A monitored at absorbance 380 nm was found to different from those of the WT. There was one phase of the C4a-(hydro)peroxyflavin intermediate formation and these were independent on reaction pHs (**Figure 7A and B**). Observed rate constants were calculated to be 68 s^{-1}. When oxygen concentration was varied, the phase increases with oxygen concentrations, suggesting the phase of oxygen reaction of Lux:$FMNH^-$ (**Figure 7C**).

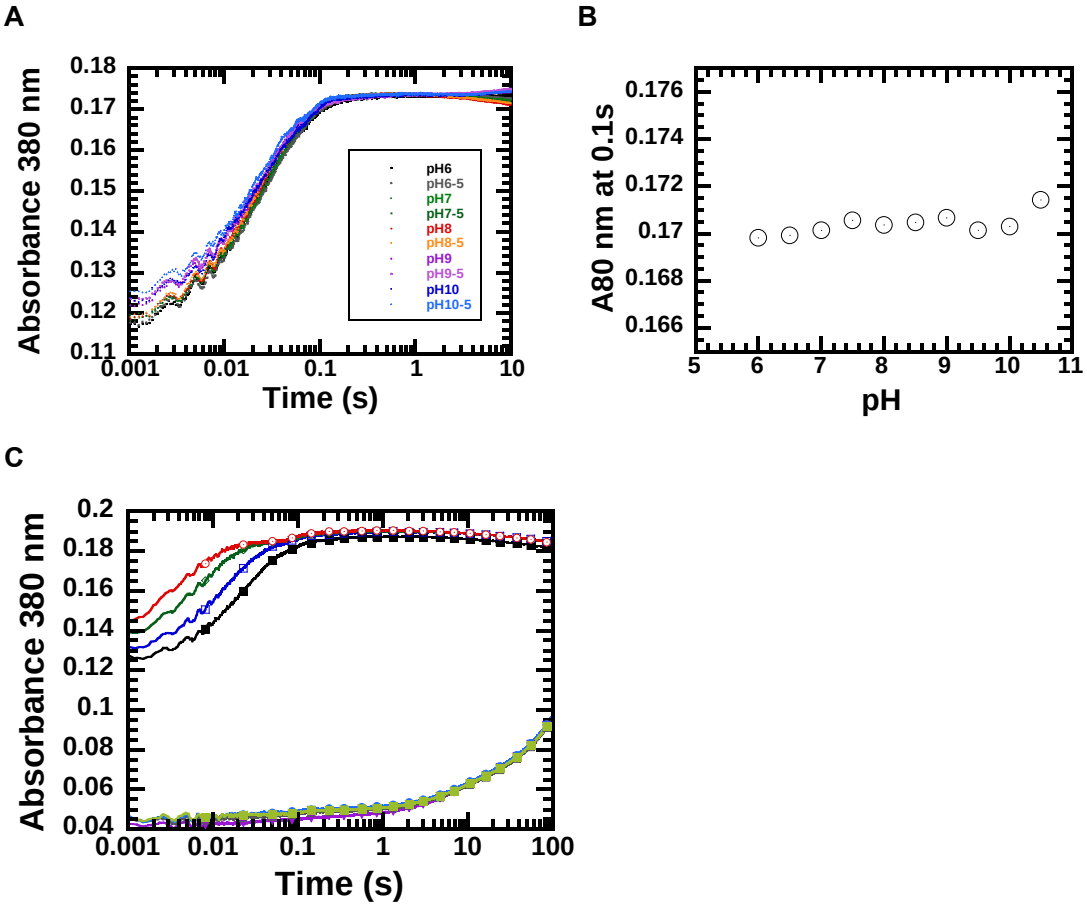

Figure 7 Lux:FMNH$^-$ and oxygen reaction at various pH values of H44A**.** Solutions of 80 μM Lux H44A and 16 μM FMNH$^-$ in 10 mM sodium phosphate buffer pH 7.0 was mixed with the oxygen (0.26 mM) in buffer at various pH values at 4°C. Concentrations are given as final concentrations after mixing. (A) The kinetic traces of absorbance 380 nm WT (B) A plot of absorbance 380 nm at 0.1 s of the first phase of A versus pHs. (C) Lux:FMNH$^-$ and oxygen reaction of WT at different oxygen concentrations (0.13, 0.3, 0.61 or 1.03 mM (from lower to upper traces)).

When the intermediated spectra determined in H44A, shown in **Figure 8A and B**, the intermediate with a λmax of 385 nm were observed at all pHs and this was totally different from found in WT reaction.

It is likely that the only intermediate in the form of what believe to be protonated form, C4a-hydroperoxide found in H44A reaction. The absorbance at 380 nm was independent to reaction pH (**Figure 8C**). This possibly explains the dim phenotype of H44A mutant, that the protonated form, C4a-hydroperoxide intermediate can not act as a nucleophile to react with aldehyde substrate for further producing the light. It may also suggest the crucial role of H44 in controlling protonation status of C4a-oxygen flavin adduct in Lux reaction.

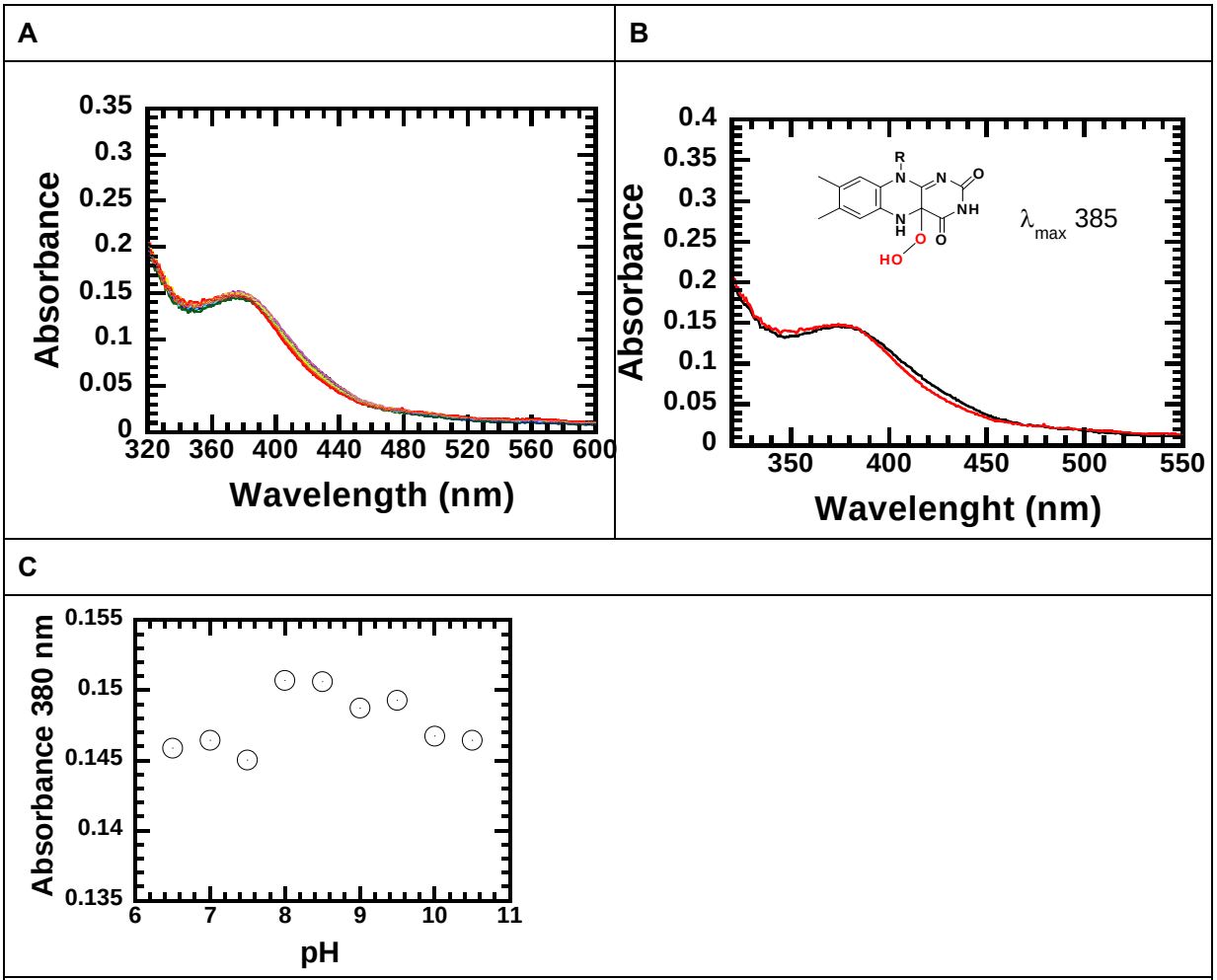

Figure 8 Spectra of the C4a(hydro)peroxyflavin of H44A at various pH values. Solutions of 80 μM Lux and 16 μM $FMNH^-$ in 10 mM sodium phosphate buffer pH 7.0 was mixed with the oxygen (0.26 mM) in buffer at various pH values at 4°C. (A and B) Intermediate spectra were detected by diod array mode attached with stopped-flow spectrophotometer. (C) Plots of absorbance change *versus* pH values.

When the effect of pH on H_2O_2 elimination was determined in H44A mutant. The observed rate constant was found to be constant at 6.5-7.5 and slightly increase with reaction pH >8. This was different to the trend found in the WT enzyme. Notably, overall, H_2O_2 elimination rate in the H44A mutant showed in the high elimination rate (0.003-0.004 s^{-1}) when compared to those of the WT. This may imply that the form of C4a-(hydro)peroxyflavin found in H44A reaction prone to be slower in FMN reoxidation reaction. The increasing in H_2O_2 elimination rate at pH>8, may be caused by enzyme structure instability in basic pH as found in the WT.

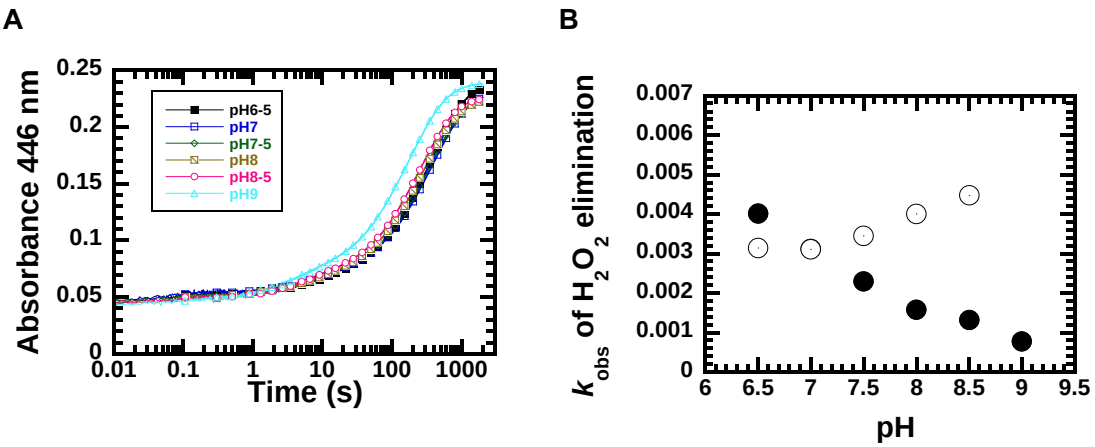

Figure 9 Effect of pH on H_2O_2 elimination in H44A enzyme. Solutions of 80 μM Lux and 16 μM $FMNH^-$ in 10 mM sodium phosphate buffer pH 7.0 was mixed with the oxygen (0.26 mM) in buffer at various pH values at 4°C and H_2O_2 elimination reaction was monitored at absorbance 446 nm (A) and (B) A plot of k_{obs} of H_2O_2 elimination as function of pH.

2.3 Effect of imidazole on oxygen reaction of H44A mutant at various pH values.

To investigate further of the function of H44 on Lux reaction. The effect of imidazole on H44A mutant reaction was investigated at pH 6.5 and 10. As the result in **Figure 10**, there were no significant different in absorbance 380 nm and 446 nm traces if the imidazole present in the H44A reaction in both pH 6.5 and 10.This suggested that the incorporation of 40 mM imidazole could not alter the C4a-(hydro)peroxyflavin formation and H_2O_2 elimination. Spectra of C4a-(hydro)peroxyflavin intermediate was also determined and no λmax shifted found in the imidazole containing reaction (**Figure 10E and F**). Overall results revealed that imidazole can not rescue intermediate in H44 reaction.

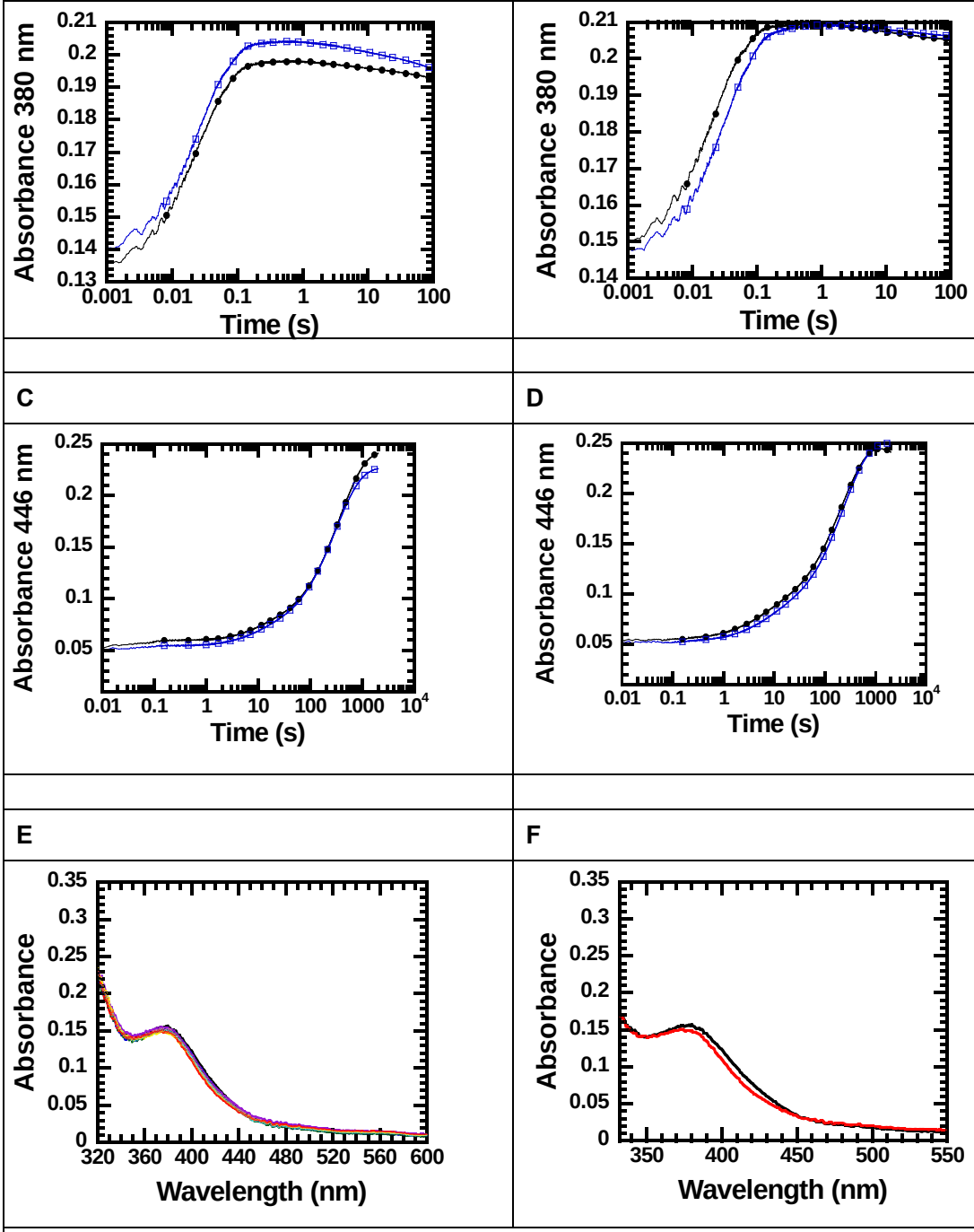

Figure 10 Comparison of the traces of absorbance 380 nm (A and B) and 446 nm (C and D) of Lux_H44A:$FMNH^-$ and oxygen reaction in the absence (black traces) and presence (blue traces) of imidazole at low and high pHs. Solutions of 80 μM Lux_H44A and 16 μM $FMNH^-$ with and without 40 mM Imidazole in 10 mM sodium phosphate buffer pH 7.0 was mixed with the oxygen (0.26 mM) in buffer at various pH values at 4°C. The reactions were monitored at absorbance 380 nm and 446 nm. (E and F) The intermediate spectra were recorded by diod array detector.

3. Discussion and conclusion

The intermediate with a λmax of 385 nm were observed at lower pH and the λmax of intermediate was shifted to shorter wavelength when reaction pH was increased, by which intermediate with a λmax of 370 nm were observed at pH 10.5. The intermediates are likely to be the flavin C4a-peroxide and C4a-hydroperoxide forms of the enzyme. It was possible that the intermediate with longer λmax found at low pH reaction may associated with the protonated form, C4a-hydroperoxide and the intermediate with shorter λmax found at high pH reaction may associated with the deprotonated form of the flavin C4a-peroxide. The changing of intermediate spectra upon changing pH values was used to determine pK_a of intermediates and found to associate with pK_a of 8.0±0.4. This value is also consistent with pK_a value calculated from the amplitude change of the first phase of absorbance 380 nm of 8.3±0.2. However, this needs further investigation.

When compare C4a-(hydro)peroxyflavin formation behaviors between pH-jump and enzyme pre-equilibrated experiments. It was found that there was no different of intermediate formation behaviors, implying the fast proton equilibration of the key control group involved in the C4a-(hydro)peroxyflavin formation at the Lux active site.

In H44A mutant, only intermediate spectra with longer λ_{max} (385 nm) were found in all pH values. It is possible that only one form of the intermediate exists in H44A active and it is likely to be the protonated form of C4a-hydroperoxyflavin intermediate. This may also suggest an implication of H44 for controlling the form of intermediates in Lux active site (**Figure 11**). However, the imidazole could not rescue H44A reaction.

pH-dependent trend of H_2O_2 elimination was also different between WT and H44A mutant. The rate of H_2O_2 elimination of WT was found to decrease upon reaction pH increased from pH 6.5-9. While in H44A, the observed rate constant was found to be constant at 6.5-7.5 and slightly increase with reaction pH >8. This may imply that the form of C4a-(hydro)peroxyflavin found in H44A reaction prone to be slower in FMN reoxidation reaction.

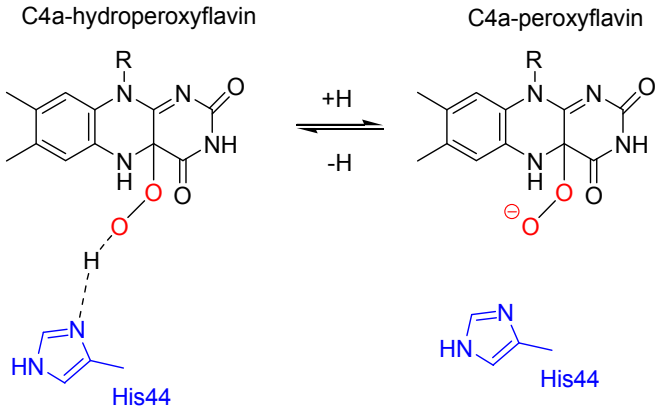

Figure 11 Implication of H44 in controlling the form of C4a-(hydro)peroxyflavin intermediates in Lux active site.

References

Shimomura, O. (2006) *Bioluminescence: Chemical principles and methods*, first ed. World Scientific Publishing Co. Pte. Ltd., Singapore, 470 pp.

Tinikul, R., Chaiyen, P. (2014) Structure, Mechanism and Mutation of Bacterial Luciferase, In: Thouand, G., Marks, R., Belkin, S. (Eds.). *Bioluminescence: fundamentals and applications in biotechnology*. Springer. (In press)

Shaw, J. J., Kado, C. I. (1986) Development of a *Vibrio* bioluminescence gene-set to monitor phytopathogenic bacteria during the ongoing disease process in a non-disruptive manner. *J. Biotechnol*. 4, 60-64.

Ulitzur, S. (1997) Review paper established technologies and new approaches in applying luminous bacteria for analytical purposes. *J. Biolumin Chemilumin*. 121, 79–192.

Loessner, M.J., Rees, C.D., Stewart, G.A.B., Scherer, S. (1996) Construction of luciferase reporter bacteriophage A511::*luxAB* for rapid and sensitive detection of viable *Listeria* cells. *App. Environ. Microb*. 2, 1133–1140.

Smartt, A.E., Xu, T., Jegier, P., Carswell, J.J., Blount, S.A., Sayler, G.S., Ripp, S. (2011) Pathogen detection using engineered bacteriophages. *Anal Bioanal Chem.* DOI 10.1007/s00216-011-5555-5.

Tinikul, R., Thotsaporn, K., Thaveekarn, W., Jitrapakdee, S., Chaiyen, P. (2012) The fusion *Vibrio campbellii* luciferase as a eukaryotic gene reporter. *Journal of Biotechnology* 162, 346-353.

Werlund-Karlsson, A., Saviranta, P., Karp, M. (2002) Generation of thermostable

monomeric luciferases from *Photorhabdus luminescens*. *Biochem. Biophys. Res. Commun.* 296, 1072-1076.

Close, D., Xu, T., Smartt, A., Rogers, A., Crossley, R., Price, S., Ripp, S., Sayler, G. (2012) The evolution of the bacterial luciferase gene cassette (*lux*) as a real-time bioreporter. *Sensors* 12, 732-752.

Palfey, B.A., McDonald, C.A. (2010) Control of catalysis in flavin-dependent monooxygenases. *Arch. Biochem. Biophys*. 493, 26-36.

Chenprakhon, P., Trisrivirat, D., Thotsaporn, K., Sucharitakul, J. Chaiyen, P (2014) Control of C4a-hydroperoxyflavin protonation in the oxygenase component of p-hydroxyphenylacetate-3-hydroxylase. *Biochemistry*. 53, 4084-4086.

Hosseinkhani, S., Szittner, R., Meighen, E.A. (2005) Random mutagenesis of bacterial luciferase: critical role of Glu^{175} in the control of luminescence decay. *Biochem. J*. 385, 575-580.

Tinikul, R., Pitsawong, W., Sucharitakul, J., Nijvipaklu, S., Ballou D.P., Chaiyen, P. (2013). The transfer of reduced flavin mononucleotide from LuxG oxidoreductase to luciferase occurs via free diffusion. *Biochemistry.* 52, 6834-6843.

Massey V. (1994) Activation of molecular oxygen by flavins and flavoproteins. *J Biol Chem*. 269, 22459-22462.

Chaiyen, P., Fraaije, M.W., Mattevi, A. (2012) The enigmatic reaction of flavins with oxygen. *Trends Biochem Sci*. 37, 373-380.

Wongnate, T., Surawatanawong, P., Visitsatthawong, S., Sucharitakul, J., Scrutton, N.S., Chaiyen, P. (2014) Proton-coupled electron transfer and adduct configuration are important for C4a-hydroperoxyflavin formation and stabilization in a flavoenzyme. *J Am Chem Soc.* 136, 241-253.

Campbell, Z.T., Weichsel, A., Montfort, W.R., Baldwin, T.O. (2009) Crystal structure of the bacterial luciferase/flavin complex provides insight into the function of the β subunit. *Biochemistry*. 48, 6085-6094.

Suadee, C., Nijvipakul, S., Svasti, J., Entsch, B., Ballou, D.P., Chaiyen, P. (2007) Luciferase from *Vibrio campbellii* is more thermostable and binds reduced FMN better than its homologues. *J. Biochem.* 142, 539-552.

Gunsalus-Miguel, A., Meighen, E.A., Nicoli, Z., Nealson, K.H., Hastings, J.W. (1972) Purification and properties of bacterial luciferase. *J. Biol. Chem.* 247, 398-404.

Szittner, R., Meighen, E. (1990) Nucleotide sequence, expression, and properties of luciferase coded by *lux* genes from a terrestrial bacterium. *J. Biol. Chem*. 265, 16581-16587.

Delong, E.F., Steinhauer, D., Israel, D., Nealsn, K.H. (1987) Isolation of the *lux* gene from *Photobacterium leiognathi* and expression in *Escherichia coli*. *Gene* 54, 203-210.

Nijvipakul, S., Wongratana, J., Suadee, C., Entsch, B., Ballou, D.P., Chaiyen, P. (2008) LuxG is a functioning flavin reductase for bacterial luminescence. *J. Bacteriol.* 190, 1531–1538.

van Berkel, W.J.H., Kamerbeek, N.M., Fraaije, M.W. (2006) Flavoprotein monooxygenases, a diverse class of oxidative biocatalysts. *J. Biotechnol*. 124, 670-689.

Ghisla, S., Massey, V. (1989) Mechanisms of flavoprotein catalyzed reactions. *Eur. J. Biochem*.181, 1-17.

Li, Z., Meighen, E.A. (1994) The turnover of bacterial luciferase is limited by a slow decomposition of the ternary enzyme-product complex of luciferase, FMN, and fatty acid. *J. Biol. Chem.* 269, 6640-6644.

Aboukhair, N.K., Ziegler, M.M., Baldwin, T.O. (1985) Bacterial luciferase: demonstration of a catalytically competent altered conformational state following a single turnover. *Biochemistry* 24, 3942-3947.

Abu-Soud, H., Mullins, L.S., Baldwin, T.O., Raushel, F.M. (1992) Stopped-flow kinetic analysis of the bacterial luciferase reaction. *Biochemistry* 31. 3807-3813.

Thorne, N., Inglese, J., Auld, D.S. (2010) Illuminating insights into firefly luciferase and other bioluminescent reporters used in chemical biology. *Chem. Biol.* 17, 646-657

Waidmann, M.S., Bleichrodt, F.S., Laslo, T., Riedel, C.U. (2011) Bacterial luciferase reporters: the Swiss army knife of molecular biology. *Bioeng. Bugs* 2, 8-16.

Sucharitakul, J., Tinikul, R., Chaiyen, P. 2014. Mechanisms of reduced flavin transfer in the two-component flavin-dependent monooxygenases. *Arch Biochem Biophys.* 555-556:33-46.

Tinikul, R., Pitsawong, W., Sucharitakul, J., Nijvipaklu, S., Ballou D.P., Chaiyen, P. (2013). The transfer of reduced flavin mononucleotide from LuxG oxidoreductase to luciferase occurs via free diffusion. *Biochemistry.* 52, 6834-6843.

Sheng, D., Ballou, D.P., and Massey, V. (2001) Mechanistic studies of cyclohexanone

monooxygenase: chemical properties of intermediates involved in catalysis. *Biochemistry*. 40,11156-1167.

Palfey, B.A., Massey, V. (1998) Flavin-dependent enzymes, in: Sinnott, M. editor. *Comprehensive Biological Catalysis, A Mechanistic Reference*. vol 3. San Deigo: Academic Press; p. 83-154.

Sucharitakul, J., Prongjit, M., Haltrich, D., Chaiyen, P. (2008) Detection of a C4a-hydroperoxy-flavin intermediate in the reaction of a flavoprotein oxidase. *Biochemistry*. 47, 8485-8490.

Prongjit, M., Sucharitakul, J., Palfey, B.A., Chaiyen, P. (2013) Oxidation mode of pyranose 2-oxidase is controlled by pH. *Biochemistry*. 52, 1437-1445.

Ruangchan, N., Tongsook, C., Sucharitakul, J., Chaiyen, P. (2011) pH-dependent studies reveal an efficient hydroxylation mechanism of the oxygenase component of p-hydroxyphenylacetate 3-hydroxylase. *J Biol Chem*. 286, 223-33.

Sucharitakul, J., Wongnate, T., Chaiyen, P. (2011) Hydrogen peroxide elimination from C4a-hydroperoxyflavin in a flavoprotein oxidase occurs through a single proton transfer from flavin N5 to a peroxide leaving group. *J Biol Chem*. 286, 16900-16909

Frederick, R.E., Ojha, S., Lamb, A., Dubois, J.L. (2014) How pH modulates the reactivity and selectivity of a siderophore-associated flavin monooxygenase. *Biochemistry*. 53, 2007-2016.

Research topic II

Probing the Ionization State of the Catalytic Cysteine in Succinic Semialdehyde Dehydrogenase from *Acinetobacter baumannii* using Burst Kinetics, NADP-Cysteine Adduct and pH-Dependent Studies

1. Introduction

Succinic semialdehyde dehydrogenase (SSADH) is an enzyme that belongs to the aldehyde dehydrogenase superfamily (ALDH Class 5). SSADH catalyzes the oxidation of SSA to succinic acid by transferring a hydride equivalent to $NAD(P)^+$ [1]. In humans, SSADH is the last enzyme in the γ-aminobutyric acid (GABA) degradation

pathway. The enzyme is important for preventing the accumulation of toxic SSA, a major metabolite from GABA catabolism. Patients with inherited SSADH deficiency exhibit neuronal toxicity symptoms that are linked to psychomotor retardation [2, 3]. Therefore, human SSADH plays an important role in preventing the neurotoxicity that might result from GABA metabolism. In bacteria, SSADH functions in the degradation pathways of GABA and *p*-hydroxyphenylacetic acid (4-HPA) [4]. The physiological role of SSADH in prokaryotes is to convert a toxic metabolic intermediate SSA into succinic acid, a common intermediate in the TCA cycle that is useful for cellular metabolism. Bioinformatic analysis of SSADH sequences has shown that this enzyme is prevalent in a wide range of organisms, substantiating its important physiological role in cell detoxification [5].

Based on cofactor specificity, SSADHs can be divided into two groups. SSADHs with a preference to use $NADP^+$ are classified as GabD orthologs, while the enzyme forms which prefer to use NAD^+ are YneI orthologs [6, 7]. GabD is encoded by the *gabD* gene that is located in the *gab* cluster which is involved in GABA degradation [1, 8]. In contrast, the *yneI* (*sad*) gene is not associated with any specific operon and resides near *yneJ* (which encodes a putative transcriptional regulator) and *yneH* (which encodes a glutaminase-2) [7]. It is thought that *yneI* may take part in SSA detoxification because it is strongly induced when SSA is accumulated. The observations of high *yneI* gene expression concomitant with overexpression of the genes related to nitrogen compound metabolism under stress conditions also suggests another physiological role of YneI in nitrogen metabolism [4,6]. Although *yneI* is not located close to any genes encoding enzymes in the 4-HPA degradation pathway, its enzyme activity has been proposed to involve SSA oxidation at the last step of the 4-HPA degradation pathway in *Escherichia coli* W [6, 9, 10]. Recently, our group has identified the first SSADH that is located in the 4-HPA degradation operon in *A. buamannii* which is an opportunistic pathogen. This enzyme participates in the last step of succinic acid production from 4-HPA degradation [5]. This pathway is of interest for investigation as it can potentially convert lignin-derived or man-made aromatic compounds into valuable bio-based chemicals such as succinic or pyruvic acid [5].

Due to the importance of SSADH physiological functions, the enzymes from several species have been investigated. SSADHs have either one or two conserved cysteines in their active sites. It was proposed that a thiolate form of the conserved cysteine acts as a nucleophile to attack SSA to generate a thiohemiacetal intermediate before the hydride is transferred to $NAD(P)^+$ in the enzyme-substrate ternary complex.

The thioester intermediate then undergoes deacylation mediated by the catalytic glutamate and an activated water molecule [11]. Enzymes with different cysteine numbers of cysteine residues are thought to use different mechanisms in the control of their activities [12-14]. In 1-cysteine SSADHs, it has been suggested that cofactor-dependent oxidation protection is the control of overall activity. However, a redox-dependent switch for regulating activity was proposed for 2-cysteine SSADHs. For a 1-cysteine SSADH from cyanobacterial *Synechococcus*, a covalent adduct formed between the catalytic cysteine (Cys262) and the C4 atom of the nicotinamide ring of $NADP^+$ was observed in its structure. Pre-incubation of the enzyme with the $NADP^+$ cofactor was also able to protect the catalytic cysteine from H_2O_2 oxidation [14]. It was thought that for the 1-cysteine system, the covalent adduct between the cysteine and $NADP^+$ is formed first, before the binding of SSA [14]. For human and *E. coli* GabD SSADHs that possess two cysteines, one cysteine is thought to act as a catalytic residue and the other is assigned as a neighboring cysteine. The reversible formation of a disulfide bond between the two cysteine residues in the catalytic loop under oxidizing conditions induced a large conformational change which resulted in enzyme inactivation [13]. It was proposed that alteration of disulfide bond forming and free cysteine thiols under oxidizing and reducing states controls enzyme activity [12, 13, 15]. However, because the pre-incubation of $NADP^+$ with *E. coli* GabD was also found to protect the enzyme from H_2O_2 dependent oxidation, the *E. coli* GabD was expected to use both mechanisms of redox-switching and NADP-adduct protection, in the control of its activity [14].

Although site-directed mutagenesis studies of SSADH were carried out, not much insight is available into the nature of the environment that controls the enzyme activity. Mutations of the conserved catalytic Cys289 in *E. coli*, Cys340 of human and Cys262 of cyanobacteria to Ala resulted in inactive enzymes [12, 14], while mutation of the neighboring cysteine in the 2-cysteine SSADH from *E. coli* decreased the enzyme activity [15]. Recent theoretical analyses of the atomic interactions within the available structures of enzymes in the ALDH superfamily suggest that the microenvironment of the ALDH active site may affect the pK_a value of the catalytic cysteine of enzymes in the ALDH superfamily [16]. However, experimental evidence to support this theoretical proposition has not been demonstrated.

Despite the fact that multiple investigations into the regulatory mechanisms of 2-cysteine SSADHs have been performed, several mechanistic issues of these enzymes remained unexplored. In particular, the precise role of the active site residues in

catalysis has not been fully addressed. The rate-limiting step in the SSADH reaction also has not been investigated. Furthermore, the key properties of the microenvironment of the SSADH active site (or those of the other ALDH Class 5 enzymes) which enhances the nucleophilicity of the catalytic cysteine is still unknown. Understanding the catalytic features which dictate the nucleophilicity of SSADH will not only contribute to knowledge on SSADH, but will also serve a broader interest of augmenting our understanding of the reaction mechanisms of other enzymes in the ALDH Class 5 family in general. This understanding will likely facilitate development of therapeutics for diseases which are associated with ALDH enzyme abnormalities. Mutation of ALDH enzymes have been showed to cause several diseases, and the overexpression of ALDHs in normal and cancer stem cells suggests that these enzymes have the potential to be used as cancer markers [17].

In this study, the catalytic reaction of 2-cysteine SSADH from *A. baumannii* (*Ab*SSADH) that is part of the 4-HPA degradation operon was investigated. Results from biochemical and biophysical characterizations of *Ab*SSADH have shown that the enzyme prefers to use $NADP^+$ as a substrate. This is the first report of $NADP^+$-preference SSADH which is not a part of the GABA pathway in bacteria. Pre-steady state kinetics using stopped-flow detection of NADPH absorbance revealed burst kinetics, implying that the hydride transfer to $NADP^+$ is faster than the following steps. As magnitude of burst kinetics represents the amount of NADPH formed during the first turnover and is directly dependent on the amount of nucleophilic cysteine thiolate, these data were used to calculate a pK_a value of Cys289. A pK_a of Cys289 was also independently measured based on the ability of thiolate cysteine to form the NADP-cysteine adduct. The pK_a values obtained from these two independent methods were compared and found to be similar to a pK_a value obtained from the pH-rate profile (7.5±0.1).

2. Objectives

2.1 To characterize biochemical properties and steady-state kinetic parameters of the SSADH.

2.2 To investigate the effect of non-catalytic cysteine residue on SSADH activity and pH rate profiles of the SSADH.

3. Materials and Methods

3.1 Reagents

All laboratory reagents used were analytical grade and mostly purchased from Sigma-Aldrich and Merck-Millipore. Molecular biology reagents, restriction endonucleases and T4 DNA ligase were purchased from New England Biolabs, high fidelity *Pfu* DNA polymerase from ThermoFisher Scientific, plasmid preparation kit and gel/PCR purification kit from Favorgen. Oligonucleotide primers were synthesized by BioBasic Inc. DNA sequences were analyzed by an automated DNA sequencing machine service of Macrogen (Korea). All chromatographic media were purchased from GE Healthcare. Protein markers for analyzing *Ab*SSADH purity were from Enzmart Biotech (Thailand). SSA for assaying SSADH activity was from Santa Cruz Biotechnology. The extinction coefficients of the following compounds were used for determining their concentrations: $NAD(P)^+$, ε_{280} = 18 $mM^{-1}cm^{-1}$; NAD(P)H, ε_{340} = 6.22 mM^{-1} cm^{-1}; wild-type SSADH from *A. baumannii*, ε_{280} = 49.64 $mM^{-1}cm^{-1}$.

3.2 Construction of the pET15b-ssadh recombinant plasmid

The *Abssadh* gene was sub-cloned into the pET15b expression plasmid. Primers were designed for the amplification of the *ssadh* gene with incorporation of an *Nco*I site:CAC GCC ATG GAA TTA AAA GAT ACA TCA TTA TTA AAA CAA C and a *Bam*HI site:CGG GAT CCT TAA ATT CCC ATA CAC ATA TAT TTG AGT TC. A nucleotide after the start codon was changed from C to G in the forward primer for generating the *NcoI* cut side **(**underlined**)** without changing of the amino acid sequence. The pBluescript plasmid-containing the 4-HPA-degradation operon of *A. baumannii* [5,42] was used as a template for polymerase chain reaction (PCR) amplification. The PCR reaction consisted of the *ssadh* template, 400 nM of each primer, 0.2 mM dNTPs and 2.5 Units of Pfu polymerase in 50 µl reactions. The PCR reaction was hot-started at 95°C for 3 min and followed by 30 PCR cycles of 95 °C for 30 s, 50 °C for 30 min and 72 °C for 3 °C. The reaction at the last cycle was extended at 72 °C for 5 min. The 1.5 kb PCR product obtained was ligated into an expression vector pET15b at the *Nco*I and *Bam*HI restriction sites. The sequence of the pET15b-*ssadh* recombinant plasmid was analyzed by Macrogen Inc., (Korea).

3.3 Construction of *Ab*SSADH variants

Two mutated *Abssadh* genes for overexpression of the variants Cys289Ala and Cys291Ala were constructed by site-directed mutagenesis. The wild-type *Abssadh*-

containing pET15b plasmid was used as a template for polymerase chain reaction (PCR) amplification. The PCR reaction consisted of the *Abssadh* template, 400 µM of each primer, 400 µM dNTPs and 2.5 Unit of *Pfu* polymerase in 50 µl reactions. The PCR reaction was hot-started with 95°C for 5 min and followed by 16 cycles of 95 °C for 45 s, 53 °C for 1 min and 72 °C for 14 min. The last reaction cycle was maintained at 72 °C for 18 min. The PCR product was treated with *Dpn*I endonuclease at 37 °C overnight before it was transformed into *E. coli* XL1 (blue) competent cells. The sequence of the mutated *Abssadh* plasmid was analyzed by Macrogen Inc., (Korea).

3.4 Expression and purification of *Ab*SSADH

The genes of pET15b-*Abssadh* wild-type and variants were transformed into *E. coli* BL21 (DE3). A colony of *E. coli* harboring pET15b-*ssadh* was inoculated into 100 ml of ZYM-5052 starter auto induction media supplemented with 50 µg/ml ampicillin and grown at 37 °C, 250 rpm for 16 h. The overnight starter culture was inoculated (1% v/v) into 4 L of ZYM-5052 medium containing 50 µg/ml ampicillin. Cells were grown at 37 °C until their OD_{600} reached ~1.0 and the culture temperature was then changed to 25°C and protein expression was allowed to proceed for another 16 h. Cells were harvested by centrifugation at 8000 rpm at 4°C for 8 min. Cells were stored at 80°C until used.

All buffers in purifying process contained 1 mM DTT. Frozen cell paste was thawed and resuspended in 50 mM sodium phosphate buffer pH 7.0 containing 1 mM DTT, 0.3 mM EDTA and 60 µM PMSF. Cells were disrupted by sonication and were then separated by centrifugation at 12,000 rpm, 4°C for 45 min. The supernatant, defined as a crude extract was precipitated by adding 0.5% polyethyleneimine (PEI). The precipitated nucleic acid was removed by centrifugation at 12,000 rpm, 4°C for 45 min. The supernatant part was precipitated by adding ammonium sulfate to 40% saturation and the protein pellet was separated by centrifugation at 12,000 rpm, 4°C for 45 min. The pellet (0-40% ammonium sulfate) was resuspended in dialysis buffer (10 mM sodium phosphate buffer pH 7.8) and the resulting protein solution was dialyzed against 4 L of dialysis buffer at 4 °C overnight. The dialyzed protein was loaded onto a DEAE-Sepharose anion exchange column which was pre-equilibrated with 10 mM sodium phosphate buffer pH 7.8. The column was then washed with 1 L of 10 mM sodium phosphate buffer pH 7.8 containing 50 mM sodium chloride and eluted with 2 L of a linear gradient of 10 mM sodium phosphate buffer pH 7.8 containing 50 to 400 mM

sodium chloride. Fractions containing *Ab*SSADH were pooled and concentrated by ultrafiltration with an Ultracel® 10 KDa (10 kDa cut off).

All protein was precipitated by 80% ammonium sulfate before being loaded onto a phenyl sepharose column which was pre-equilibrated with sodium phosphate buffer pH 7.8 containing 20% (w/v) ammonium sulfate. The column was then washed with 500 ml of 50 mM sodium phosphate buffer pH 7.8 containing 8 % (w/v) ammonium sulfate and eluted with 1 L of a linear gradient of 8 % to 0 % (w/v) ammonium sulfate in 50 mM sodium phosphate buffer pH 7.8. Fractions containing *Ab*SSADH were pooled and exchanged into 50mM sodium phosphate buffer pH 7.8 containing 1 mM DTT, 0.5 mM EDTA and 10% glycerol before being kept at-80°C until used.

The native molecular mass of the recombinant enzyme was determined using gel filtration chromatography on a Superdex S-200 10/300 column run on an AKTA FPLC system (GE Healthcare). The protein molecular weight standards used were ferritin (440 kDa), amylase (200 kDa), alcohol dehydrogenase (150 kDa), bovine serum albumin (BSA; 65.4 kDa), carbonic anhydrase (29 kDa) and cytochrome C (12.4 kDa). Blue dextran was used to determine the void volume, and FAD was used for determination of the late retention volume. All samples were eluted with 50 mM sodium phosphate pH 7.0 containing 150 mM NaCl at 25^{o}C with a flow rate of 0.5 ml/min and the absorbance was monitored at 280 nm.

3.5 Enzyme activity assay

Activity of *Ab*SSADH was measured based on the production of NAD(P)H which can be monitored by absorbance at 340 nm. Assay reactions typically consisted of 20 nM SSADH, 0.60 mM SSA and 0.75 mM NAD(P)$^{+}$ in 50 mM sodium phosphate buffer pH 8.0 with 1 mM DTT. The enzyme reaction was initiated by adding *Ab*SSADH into the reaction mixture and NAD(P)H production was measured using spectrophotometry. The initial velocity of the SSADH reaction was calculated from the initial slopes of the assay. The, specific activity (unit/mg protein) was then calculated. One unit of SSADH is defined as the amount of enzyme that catalyzes the formation of 1 μmol of NAD(P)H per min at 25^{o}C. To test the suitability of buffers for SSADH, SSADH activity was assayed in 5 different buffer types including (1) 50 mM sodium phosphate buffer pH 8.0, (2) 50 mM potassium phosphate buffer pH 8.0, (3) 50 mM Tris/HCl pH 8.0, (4) 50 mM MOPS buffer pH 8.0 and (5) 50 mM HEPES buffer pH 8.0. SSADH activity was assayed with NAD^{+} or NADP^{+} to investigate SSADH electron acceptor preference.

3.6 Quantitative determination of the reactive cysteine in *Ab*SSADH

The number of reactive cysteines in the *Ab*SSADH variant were quantitatively determined for both the reduced and oxidized states. To generate the reduced state of *Ab*SSADH, the purified enzymes (wild-type and mutants) were reduced by pre-incubating with 1 mM DTT, while the oxidized state was prepared by pre-incubating wild-type enzyme with 1 mM H_2O_2. Then, excess DTT or H_2O_2 were removed by passing the solutions through a PD-10 column. The reactive cysteines in both states of *Ab*SSADH were determined by reacting with DTNB.

*Ab*SSADH wild-type and variants were mixed with 0.1 mM Ellman's reagent in 0.1 M sodium phosphate buffer pH 8 containing 1 mM EDTA. After the reaction was initiated by adding Ellman's reagent, the reaction was incubated at room temperature in the dark for 1 h. TNB^{2-} production was then measured by absorbance at 412 nm. Negative control reactions with only 0.1 mM Ellman's reagent or *Ab*SSADH were used as blanks. An extinction coefficient of TNB^{2-} of 14,150 M^{-1} cm^{-1} was used to determine the number of reducing thiols contained within *Ab*SSADH [43]. To calculate the number of *Ab*SSADH reactive thiol groups, the absorbance values for SSADH samples reacted with Ellman's reagent with the absorbance of the blank subtracted were used.

3.7 Effect of pH on *Ab*SSADH activity

The effect of pH on *Ab*SSADH activity was investigated by measuring the enzyme activity at various pH values using methods described previously [44, 45]. A 10 mM sodium phosphate buffer was used for maintaining the pH between 6-8.5, while a pH between 8.5-10.5 was maintained with 10 mM sodium pyrophosphate. The ionic strengths of both buffers were kept constant at 0.1 M. The specific activity was plotted as a function of pH. The pK_a value for the enzyme was analyzed according to Equation 1, where Y is the apparent maximum velocity; C is the pH independent value of V_{max}, and K_a is the dissociation constant of the ionizable group.

$$Y = \frac{C}{1+10^{-pH}/10^{-pKa}} \qquad \text{(Eq. 1)}$$

3.8 Steady-state kinetics of *Ab*SSADH

The steady state kinetics of *Ab*SSADH were investigated by varying the concentrations of the two substrates. Initial velocities of the SSADH reaction with various concentrations of SSA (20, 40, 80, 320, 400 and 640 μM) and $NADP^+$ (5, 20, 40, 80, 320 and 640 μM) were investigated in 50 mM sodium phosphate buffer pH 8 with 1 mM DTT at 25 °C. The initial slopes of the assay reaction were calculated using Program A (developed by Chun-Jen Chiu, Rong Chang, Joel Dinverno, and David P. Ballou, University of Michigan, Ann Arbor, MI, USA). Double-reciprocal plots were used to identify the type of reaction mechanism according to Dalziel's equation (Equation 2). Steady-state kinetic parameters were analyzed using EnzFitter program according to Equation 3 (Biosoft, Cambridge, UK).

$$\frac{\varepsilon}{v} = \mathcal{Q}_0 + \frac{\mathcal{Q}_A}{[A]} + \frac{\mathcal{Q}_B}{[B]} + \frac{\mathcal{Q}_{AB}}{[AB]} \qquad \text{(Eq. 2)}$$

$$V = \frac{V_{max}[A][B]}{K'_{IA}K_B + K'_A[B] + K_B[A] + [A][B]} \qquad \text{(Eq. 3)}$$

3.9 Pre-steady-state kinetics of *Ab*SSADH

The burst kinetics of $NADP^+$ reduction in the SSADH reaction was investigated by monitoring the absorbance at 340 nm using a single-mixing stopped-flow spectrophotometer at 4 °C. To slow down the reaction to obtain clear burst phase, the enzyme reaction was performed at 4°C. The reaction was conducted in 50 mM sodium phosphate buffer pH 8.0 containing 1 mM DTT. A solution of SSA and $NADP^+$ was mixed with a solution of SSADH to a final concentration of 200 μM SSA, 300 μM $NADP^+$ and 5 and 10 μM of wild-type in the stopped-flow spectrophotometer apparatus. NADPH production was followed by monitoring the increase in absorbance at 340 nm. All concentrations are reported as final concentrations. The amplitude of the burst phase representing NADPH production was calculated by extrapolation of the steady-state rate to time zero-using Equation 4.

$$A = A_0(1 - e^{-k_{obs}t}) + v_{ss}t + C \qquad \text{(Eq. 4)}$$

In Equation 4, A is the observed absorbance at 340 nm at time t, A_0 is the absorbance change during the burst phase due to NADPH generation, v_{ss} is the steady-state turnover rate under these conditions and C is compensate for the nonzero baseline. The NADPH concentration during the first turnover can be directly calculated from the value of the burst, A_0/ε_{340}. ε_{340} is the absorption coefficient of NADPH at 340 nm (6.22 $mM^{-1}cm^{-1}$). The pH effects on the burst kinetics were investigated by measuring the magnitude of the burst phase in buffers of different pH values with 0.1 M buffer ionic strength using 10 mM sodium phosphate buffer for pH maintenance from 6.0-8.5 and 10 mM sodium pyrophosphate for pH maintenance from 8.5-10.5. The final pHs were used for plotting the pH dependent profiles.

3.10 Formation of an NADP-cysteine adduct at various pHs

An NADP-cysteine adduct formation was investigated using spectrophotometry. Spectra of mixtures SSADH (200 μM) and $NADP^+$ (200 μM) in buffer with various pH values containing 1 mM DTT were recorded at 200 to 800 nm at 25°C every 10 min for 1 h. The 0.1 M buffer ionic strength of 10 mM sodium phosphate and 10 mM sodium pyrophosphate buffers were used to maintain pH as described previously. Final pH values were used for plotting pH-dependent rate profiles.

4. Results

4.1 Sequence analysis of *Ab*SSADH reveals its high degree of sequence similarity to other enzymes in the two-cysteine GabD family

The sequence of *AbSSADH* which contains 482 amino acids has the highest sequence identity (62%) to SSADH encoded by the *gabD* gene that is part of the GABA degradation pathway in *E. coli* (GI: 147901) (GabD). Sequence analysis of *Ab*SSADH and its homologues using the Enzyme Function Initiation (EFI) software has shown that these enzymes are prevalent in a wide range of organisms [5]. *Ab*SSADH contains Cys289 and Cys291 as the two conserved active site cysteines (Fig. 1) which are equivalent to Cys289 and Cys291 in the *E. coli* GabD. As the *ssadh* gene from *A. baumannii* is part of the 4-HPA degradation pathway in which SSADH converts SSA to succinic acid before entering the main metabolic TCA cycle [5, 18], this is the first report to demonstrate the existence of a member of the SSADH GabD family outside the GABA degradation operon.

A

			% identity
A. baumannii	279	ASKFRNSGQT**C**V**C**TNRLLVQAS 300	100
GabD_*E.coli*	279	ASKFRNAGQT**C**V**C**ANRLYVQDG 300	62
GabD_*R.norvegicus*	318	ASKFRNAGQT**C**V**C**SNRFLVQRG 339	56
GabD_*H. sapiens*	330	ASKFRNTGQT**C**V**C**SNQFLVQRG 351	57
YneI_*B. subtilis*	256	ASKYRNAGQT**C**V**C**ANRLIVHES 277	55
GabD_*M. tuberculosis*	255	TGRVQNNGQS**C**IAAKRFIVHAD 276	32
GabD_*S. pyogenes*	253	FSRLYNAGQV**C**TSSKRFIVLDK 274	28
YneI_*S. typhimurium*	258	AGRYQNTGQV**C**AAAKRFIVEEG 279	31
YneI_*E. coli*	258	AGRYQNTGQV**C**AAAKRFIIEEG 279	30

B

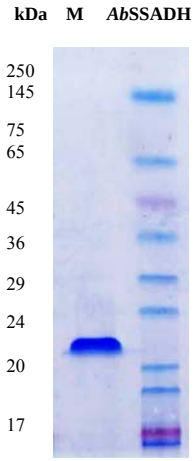

Fig. 1. Comparison of SSADH amino acid sequences from several species. (A) The sequence alignment shows that SSADHs have one or two conserved cysteines in their active sites. SSADH sequences were retrieved from the National Center for Biotechnology Information (NCBI): GabD from *Escherichia coli* (GI: 147901), GabD from *Rattus norvegicus* (GI: 449784888), GabD from *Homo sapiens* (GI: 4507229), YneI from *Bacillus subtilis* (GI: 16077459), GabD from *Mycobacterium tuberculosis* (GI: 358230540), GabD from *Streptococcus pyogenes* (GI: 383493878), YneI from *Samlonella typhimurium* (GI: 16764869) and YneI from *E. coli* (GI: 3915524). The catalytic cysteine residues are indicated by gray highlights. The pink highlights indicate neighboring cysteine residues of the conserved cysteine pairs. (B) SDS-PAGE analysis (15%) of purified SSADH. M = AccuProtein Chroma markers (Enzmart Biotech, Thailand) and *Ab*SSADH = 20 μg purified *Ab*SSADH.

4.2 Overexpression and purification of *Ab*SSADH

*Ab*SSADH was overexpressed in *E. coli* BL21 (DE3) cells using an auto-induction system at 25 °C for 16 h and purified according to the protocol described in Materials and Methods. After passing through four steps of purification, the enzyme was purified 3.8-fold to obtain 20% protein yield with a specific activity of 120 unit/mg (Table S1). The enzyme purity as judged by 12% SDS-PAGE was >95% (Fig. 1). Based on protein concentration measurements using the Bradford method, approximately185 mg of purified *Ab*SSADH was obtained from 1 L of cell culture. The subunit molecular mass of *Ab*SSADH was estimated to be ∼52 kDa, which is consistent with the predicted subunit molecular mass value calculated from the amino acid sequence. The native form of *Ab*SSADH as analyzed by gel filtration chromatography (Experimental Procedure) was determined as a homotetramer (data not shown).

*Ab*SSADH activity was found to decrease after the Phenyl-Sepharose purification step and two distinct peaks of SSADH activity were identified. These results were similar to those reported for SSADH from *Aspergillus niger* [19]. The enzyme in the first peak fraction showed higher SSADH activity than the one in the second peak. We also found that the SSADH activity could also be restored if dithiothreitol (DTT) was added after or included in the assay buffer, indicating that the reducing agent (DTT) can preserve the active form of *Ab*SSADH. These results also indicate that an active thiol of a cysteine residue is required for the enzyme activity.

The stability of *Ab*SSADH in various buffers was tested over time and the enzyme was found to be more stable in phosphate buffer at basic pHs. However, the activity promptly decreased in Tris buffer. The Tris-inhibition phenomenon was also found in other SSADHs such as the enzymes from *E. coli* and potato [4, 20]. This is possibly due to the reaction of a Tris amine group with an aldehyde moiety of SSA to generate an imine Schiff base which prevents formation of the enzyme-SSA adduct that is required for SSADH catalysis.

4.3 Preference of a hydride acceptor for *Ab*SSADH

SSADHs have been classified according to their cofactor preference. In *E. coli*, there are two types of SSADHs. The first type is GabD which is an $NADP^+$-dependent SSADH, and the second type is YneI which either has the same preference for NAD^+ and $NADP^+$ or prefers NAD^+ more than $NADP^+$ [4, 6]. We investigated the hydride acceptor preference of *Ab*SSADH by assaying the enzyme activity using $NADP^+$ and NAD^+ as co-substrates. The results showed that *Ab*SSADH can use both $NADP^+$ and NAD^+ as electron acceptors but has more preference towards $NADP^+$. The specific activity of the enzyme with $NADP^+$ was found to be 10 times higher than that for the reaction using NAD^+ (Fig. 2A). These results also indicate that *Ab*SSADH is more closely related to the *E. coli* GabD than its functional ortholog YneI, in agreement with the sequence similarity analysis (Fig.1).

A previous investigation on the cofactor and substrate selectivity of *Synechococcus* SSADH has shown that the cofactor preference is determined by specific residues in the cofactor binding pocket of SSADH [21]. Thus, the residues that may be involved with cofactor selectivity in *Ab*SSADH were identified based on the sequence alignment of GabDs and YneIs (Fig. 2B). At the position which may be involved in NAD(P) binding, Ser183 was found in *Ab*SSADH, which is equivalent to Ser183 in GabD. In the YneI ortholog, proline is found instead of serine. An *Ab*SSADH homology model was built based on the aldehyde dehydrogenase X-ray structure (PDB:3EK1) which has the highest sequence similarity to *Ab*SSADH. The overlay of this *Ab*SSADH structural model with *E. coli* GabD and *Salmonella typhimurium* YneI complexes with $NADP^+$ confirmed that the phosphate group of $NADP^+$ possibly binds around the Ser183 pocket area (Fig. 2C).

A

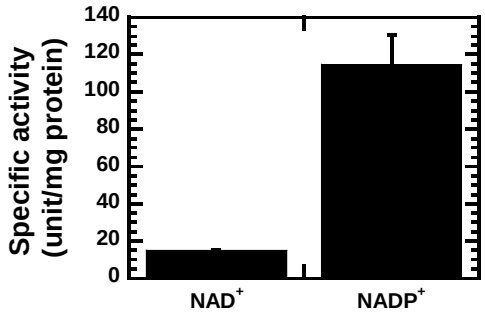

B

Species	Critical position of cofactor recognition	Cofactor preference
SSADH *A. baumannii*	173 AGCTVIIKPASETPLSAFALA 193	$NADP^+$
YneI_*E. coli*	153 AGNGYLLKHAPNVMGCAQLIA 173	equally
YneI_*B. subtilis*	150 AGCTFIIKPAPDTPLSAYELA 170	equally
YneI_*S. typhimurium*	153 AGNSYLLKHAPNVTGCAQMIA 173	NAD^+
GabD_*E. coli*	173 AGCTMVLKPASQTPFSALALA 193	$NADP^+$
GabD_*M. tuberculosis*	150 AGNVGLLKHASNVPQCALYLA 170	$NADP^+$
GabD_*S. pyogenes*	148 VGNPMVLKHASICPRSAQSFE 168	$NADP^+$

C

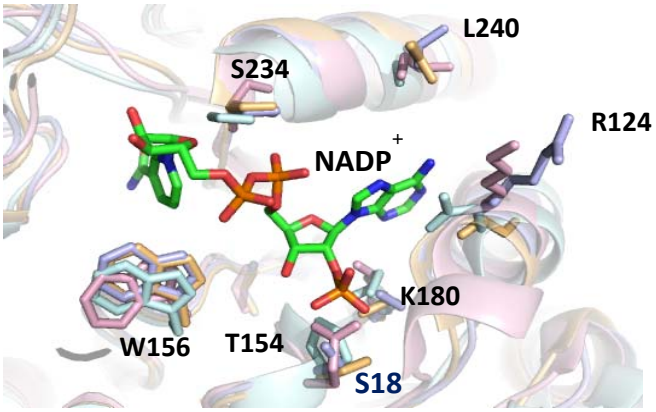

Fig. 2. (A) Cofactor preference of *Ab*SSADH. (B) Alignment of amino acids involved in cofactor recognition of *Ab*SSADH and SSADHs from various organisms. The critical position of cofactor recognition is indicated by light gray highlight. (C) The superimposed structure of the cofactor binding pocket between the modeled structures of *Ab*SSADH (light blue), *E. coli* GabD (light orange) (PDB:3JZ4), *S. typhimurium* YneI (pale cyan) (PDB:3EFV) and *Homo sapiens* (light pink) (PDB:2W80). The structural model of *Ab*SSADH was built by SWISS-MODEL Workspace based on the aldehyde

dehydrogenase X-ray structure (PDB:3EK1) with the quality model assessment QMEAN6 of -0.95 [46].

4.4 Two-substrate steady-state kinetics of *Ab*SSADH

Two-substrate steady-state kinetics of *Ab*SSADH was investigated at 25^{o}C, pH 8.0 according to the protocol described in the Experimental Procedure. Initial velocities of the reactions were calculated from the slopes of the plots of NADPH production vs time and the data are presented as direct and double-reciprocal plots (Fig. 3A and 3B). Substrate inhibition was observed in the *Ab*SSADH reaction at SSA concentrations higher than 500 μM (data not shown). A plot of e/*v* (reciprocal of activity) *versus* 1/[SSA] at various $NADP^+$ concentrations showed a series of convergent lines, suggesting that the reaction proceeds via a mechanism that involves formation of a ternary complex. These data suggest that both SSA and $NADP^+$ must bind to the active site before the catalytic reaction can be initiated. This is similar to the rat brain SSADH [22]

Analysis of steady-state kinetic parameters by double-reciprocal plots using Dalziel's equation and direct plots using the EnzFitter Biosoft program, yielded kinetic parameters as follows: K_m^{SSA} = 189±31 μM, K_m^{NADP+} = 113±18 μM and k_{cat}= 137±9 s^{-1}. The K_m of SSA for *Ab*SSADH was 18 and 4-fold higher than those of *E. coli* GabD (10.1 μM) and YneI (46.8 μM), respectively [23]. However, *Ab*SSADH showed a distinguishingly high k_{cat} value (137±9 s^{-1}) compared to GabD from *Mycobacterium tuberculosis (*4.7 s^{-1}*)*, *Streptococcus pyogenes* (7.2 s^{-1}) and *S. typhimurium* YneI (55 s^{-1}).

Product inhibition was also investigated using substrate concentrations of 0.6 mM for SSA and 0.75 mM for $NADP^+$ in assay reactions. Product inhibition by succinic acid (at concentrations of up to 100 mM) was not observed, while NADPH inhibition started to become apparent at the 100 μM concentration. Overall, *Ab*SSADH exhibits the highest catalytic turnover (k_{cat}) and lowest susceptibility to SSA (substrate) and succinic acid (product) inhibition among all of the SSADHs previously reported. These findings suggest that *Ab*SSADH has many promising properties that can be used in biotechnology applications.

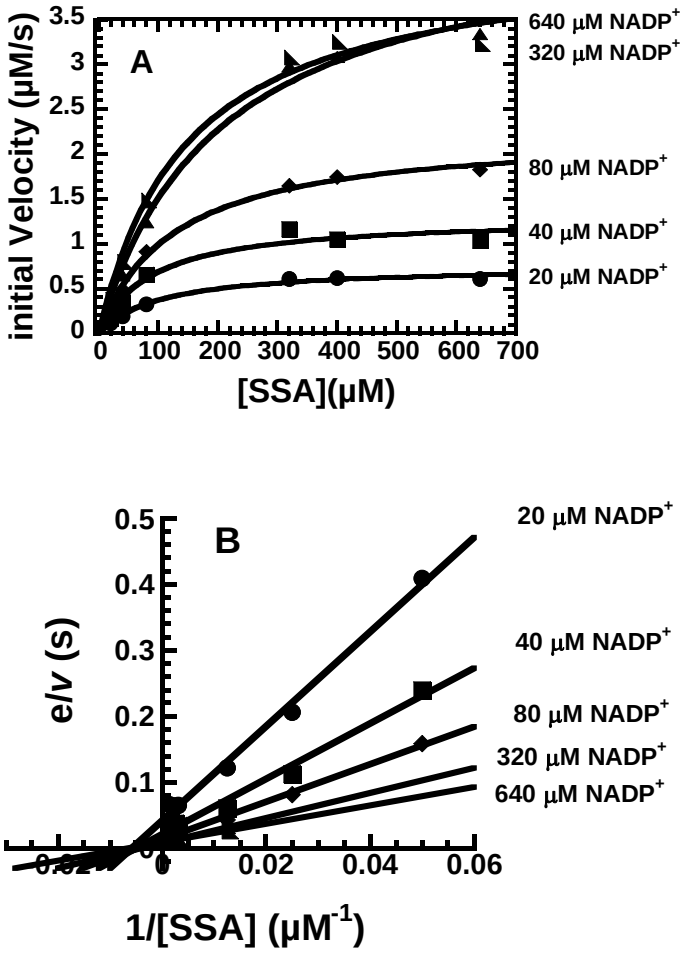

Fig. 3. (A) Direct and (B) double-reciprocal plots of the initial rates of the *Ab*SSADH reaction *versus* various SSA and $NADP^+$ concentrations. Initial velocities of *Ab*SSADH were measured using various concentrations of SSA (20, 40, 80, 320, 400 and 640 μM) and $NADP^+$ (20, 40, 80, 320 and 640 μM) at 25°C in 50 mM sodium phosphate pH 8.0 containing 1 mM DTT.

4.5 Detection of active cysteine residues and other free thiol groups in *Ab*SSADH using Ellman's reagent

As the reaction mechanism of SSADH is proposed to involve an initial nucleophilic attack by an active site cysteine, we first investigated the status of free and active thiols in the active site of *Ab*SSADH. *Ab*SSADH contains a total of five cysteine residues in one subunit (Cys175, Cys245, Cys289, Cys291 and Cys479) and the redox status of each residue is unknown. Based on sequence homology with *E. coli* GabD in which the structure is known (PDB:3JZ4), the residues Cys75 and Cys245 of *Ab*SSADH were found to be located in the cofactor binding domain, Cys289 and Cys291 in the catalytic domain and Cys479 in the oligomerization domain [13]. In order to measure the number of active cysteines in *Ab*SSADH, Ellman's reagent was used to measure the number of free thiol groups in *Ab*SSADH. The results (Table 1) showed that Ellman's reagent detected three free thiols in *Ab*SSADH. The detection of only three thiols among five cysteines in *Ab*SSADH may be due to inaccessibility of buried reactive thiols to the reagent [24] or suggests that two of the cysteines form a disulfide bond that cannot react with Ellman's reagent.

In order to identify the cysteine residues that give rise to the active free thiol signal upon reacting with Ellman's reagent, the two cysteines at the active site of *Ab*SSADH were mutated to alanine to construct the Cys289Ala and Cys291Ala variants (Table 1). The results showed that mutation of only one residue was enough to cause the loss of signal for two free thiols in the variants. These data indicate that two out of three reactive cysteines detectable by Ellman's reagent in the wild-type enzyme come from the conserved cysteine pair (Cys289 and Cys291) and that one active site thiol is important for the reactivity of another one. In order to confirm that the two active cysteines are located in close proximity to each other, *Ab*SSADH was treated with H_2O_2 to allow nearby cysteines to be oxidized and form a disulfide linkage. The results indicated that H_2O_2-pretreated wild-type *Ab*SSADH only gave signal corresponding to one reactive cysteine (Table 1). These data suggest that two out of three cysteines that can react with Ellman's reagent are located close to each other i.e. they are the conserved cysteines (Cys289 and Cys291).

Table 1 Quantitative determination of reactive cysteine residues in wild-type and variants of *Ab*SSADH using Ellman's reagent

***Ab*SSADH**	**Total cysteine residues in *Ab*SSADH**	**Number of reactive cysteines per *Ab*SSADH subunit**
1. Wild-type	5	3.0±0.0
2. Cys289Ala	4	1.5±0.0
3. Cys291Ala	4	1.2 ±0.1
4. H_2O_2 treated wild -type	5	1.6±0.1

4.6 Burst kinetics of the *Ab*SSADH reaction: evidence for rapid formation of NADPH

Single mixing stopped-flow experiments were used to investigate whether formation of NADPH during the first turnover is faster than rest of the reactions during the steady-state period. According to the mechanism proposed, a hydride transfer from the thiohemiacetal to $NADP^+$ is supposed to occur before the thioester intermediate is hydrolyzed to generate the free enzyme. If the hydride transfer to generate NADPH is faster than the following steps of deacylation and product release, burst kinetics for NADPH formation should be observed. The stopped-flow experiment (Experimental Procedure) that measured NADPH generation by monitoring absorbance at 340 nm at 4°C showed burst kinetics for NADPH production around 0.01 s before enzyme turnovers in the steady-state period began (Fig. 4). The burst magnitude and steady-state rate under these conditions were dependent on the concentrations of *Ab*SSADH (Fig. 4). The amount of NADPH produced during the burst phase of the enzyme was calculated (using Equation 4, Experimental Procedure) to be 1.0±0.02, 1.6±0.14 and 3.2±0.2 μM when the amount of *Ab*SSADH utilized of 2, 4 and 8 μM, respectively. The steady-state rate of NADPH production (using Equation 4) also increased as the *Ab*SSADH amount was increased (Fig. 4). We noted that the NADPH produced during the burst phase was lower than the total enzyme concentration used. This might be because the enzyme was not fully ionized to be the active thiolate form at this pH (see following sections) or not all the enzyme was present as the ready-to-burst ternary complex. The active form of enzyme is thus less than the total enzyme concentration. However, the NADPH produced during the burst phase under this condition was directly proportional to the enzyme used in reaction. The detection of burst signals during the

first catalytic cycle of *Ab*SSADH indicates that all reactions up to the generation of NADPH can occur rapidly at the first turnover and these steps are not the rate-limiting step. The rate-limiting step lies after the hydride transfer to $NADP^+$ and occurs either at deacylation or product release. This is the first detection of a burst phase of NADPH formation among all SSADHs and ALDH Class5 enzymes.

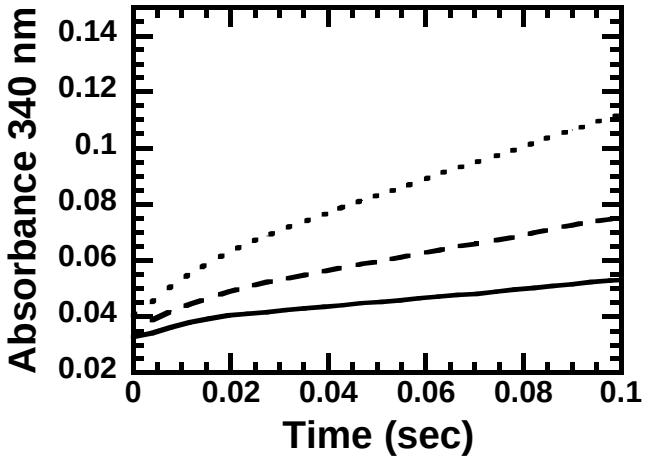

Fig. 4. Burst kinetics of NADPH generated in the *Ab*SSADH reactions. Reactions contained 200 μM SSA and 300 μM $NADP^+$ and 2 μM (solid line), 4 μM (dashed line) and 8 μM (dotted line) enzymes. The reactions were monitored using the stopped-flow spectrophotometer at 4°C at pH 8.0. NADPH production was monitored by measuring the absorbance at 340 nm. All concentrations are given as final concentrations.

4.7 pH-rate profiles of *Ab*SSADH

The pH-rate profiles of the *Ab*SSADH enzyme were investigated to probe the protonation/deprotonation status of a key residue required for activity and controlling the rate-limiting step of the reaction. The pH activity profile showed a trend towards increasing enzyme activity with an increase of reaction pH (Fig. 5). These results imply that deprotonation of ligand or active site residue is required for the SSADH reaction. The pK_a value of the group that must be deprotonated in order to achieve the higher activity was found to be 7.5±0.1 for the enzyme (Fig. 5).

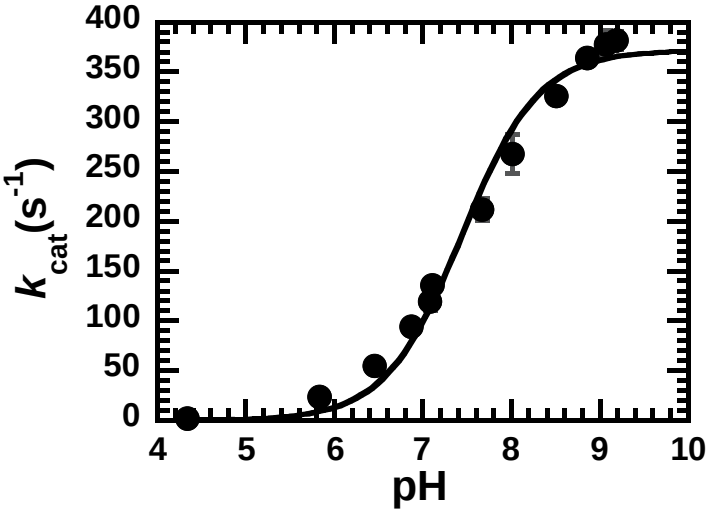

Fig. 5. pH-rate profiles of *Ab*SSADHs. Assay reactions were performed at different pHs using 0.6 mM, SSA 0.75 mM $NADP^+$ and 20 nM *Ab*SSADH**.** Catalytic turnovers are plotted as a function of pH. The pK_a value of the group that has to be deprotonated in order to achieve the higher activity was found to be 7.5±0.1.

4.8 Use of burst kinetics at various pHs as a means to measure pK_a of catalytic cysteine

As the active site cysteine should be in the thiolate form in order to initiate formation of the thio-hemiacetal intermediate (Fig. 6), we suspected that the pH-rate dependence behavior in Fig. 5 might be due to the ionization state of the catalytic cysteine. The attempt to measure a pK_a value of the catalytic cysteine directly using Ellman's reagent was not successful because of large interference from other cysteines. Because *Ab*SSADH possesses two adjacent cysteines in the active site, Cys289 and Cys291, we first identified which residue is necessary for activity and responsible for

burst phase formation using site-directed mutagenesis studies. The results showed that the Cys289Ala activity was lost while the Cys291Ala variant retained the activity to about 65% of the wild-type enzyme (data not shown). The Cys291Ala variant also showed similar burst kinetics as in the wild-type enzyme. Altogether, these results clearly indicate that Cys289 is the catalytic cysteine and is the residue responsible for NADPH production during burst kinetics.

As the SSADH reaction was proposed to be involved with the catalytic cysteine nucleophilic attack to the SSA substrate before hydride is transferred to $NADP^+$, we thus hypothesized that the NADPH production at the first catalytic cycle (shown in Fig. 4) might potentially be used to assess the thiolate cysteine amount that is directly responsible for NADPH production. The magnitude of the burst phase (Fig. 4) represents the amount of NADPH produced during the first turnover and it is directly dependent on the thiolate form of the catalytic Cys289 that can promptly react with SSA. The amount of NADPH produced during the first turnover thus represents the amount of thiolate Cys289 present. Therefore, pH effects on the burst magnitude of the enzyme reaction were investigated to study ionization state of the catalytic residue, Cys289.

When the pH of the reaction was increased from 6.0 to 9.5, the amount of NADPH formed during the burst period increased. This is likely due to greater ionization of Cys289 to the thiolate form which can subsequently generate more of the thiohemiacetal adduct that leads to more formation of NADPH during the burst phase. Therefore, the amplitude of the burst phase directly correlates with the formation of the Cys289 thiolate and these data can be used to calculate the pK_a values of catalytic Cys289 in the *AbSSADH* enzymes (Fig. 7). Note that at pH values greater than 9.0, the reaction could not be analyzed because *Ab*SSADH was denatured. A plot of the magnitude of the burst phase of the wild-type enzyme as a function of pH showed a pK_a value of 7.4 ± 0.2.

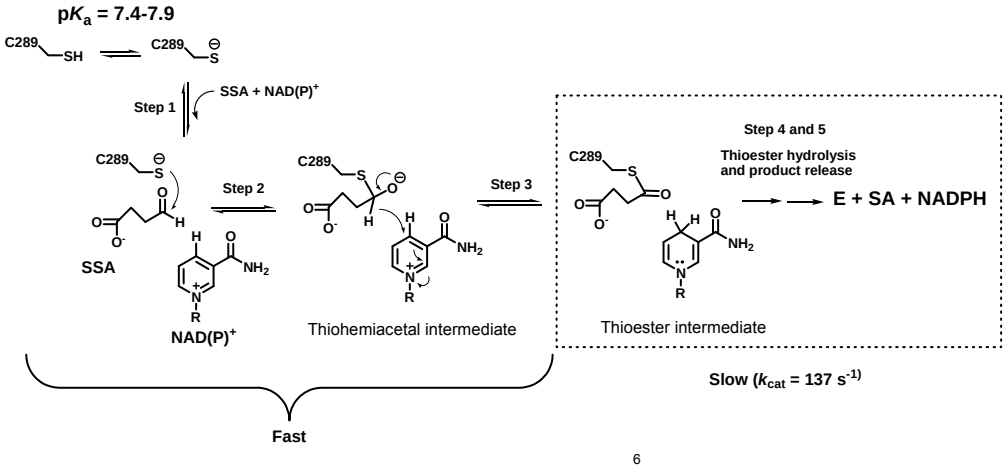

Fig. 6. Proposed reaction mechanism of *Ab*SSADH.

4.9 Use of an NADP-cysteine adduct formation at various pHs as an independent method to measure pK_a of the catalytic Cys289

To independently measure pK_a of Cys289, we used the ability of the catalytic Cys289 to form an NADP-cysteine adduct to probe the residue ionization state. Previously, the X-ray structure of SSADH from *cyanobacterial* SSADH has been found to form the NADP-cysteine adduct [14, 25].

In order to quantitate the amount of NADP-cysteine adduct formed, experiments were set up to measure spectroscopic signals of the adduct. Solutions containing *Ab*SSADH (200 μM) and NADP$^+$ (200 μM) were mixed and their spectra were compared to those of free *Ab*SSADH or NADP$^+$ in 50 mM sodium phosphate buffer pH 8 containing 1 mM DTT. Formation of the adduct could be detected by an increase of absorption ~330 nm which was not found in free solutions of *Ab*SSADH or NADP$^+$ (Fig. 8A). This species was confirmed to indeed belong to the NADP-cysteine adduct because the absorption band ~330 nm could not be detected when the Cys289Ala variant was incubated with NADP$^+$ (Fig. 8A Inset). The adduct resulting from mixing 200 μM *Ab*SSADH and 200 μM NADP$^+$ was further isolated using a G25 gel filtration column and the results showed that the species with absorption at ~330 nm was co-eluted with protein but not small molecule fractions, indicating that the absorption at ~330 nm has protein content (Fig. 8B). All together, these data indicate that we can use absorption at ~330 nm to represent the amount of NADP-cysteine adduct formed. Because formation

of the adduct is enhanced when Cys289 is in the thiolate form, the adduct formation thus was used to probe the ionization state of Cys289.

Formation of NADP-cysteine adduct in *Ab*SSADH was investigated at various pHs and the results showed that more absorption occurred at higher pHs. After incubation of 200 μM $NADP^+$ and 200 μM *Ab*SSADH at 25°C, the absorbance at 330 nm increased with time and reached saturation at around 30 min. Therefore, the absorption change after 30 min incubation at various pHs from pH 6-8.5 was used to probe the Cys289 ionization from thiol to thiolate form. The absorption increase was plotted as a function of pH to calculate the Cys289 pK_a as 7.9±0.2 (data not shown). This pK_a value is comparable to values obtained from pH-rate profile and burst kinetics measurement in the previous sections.

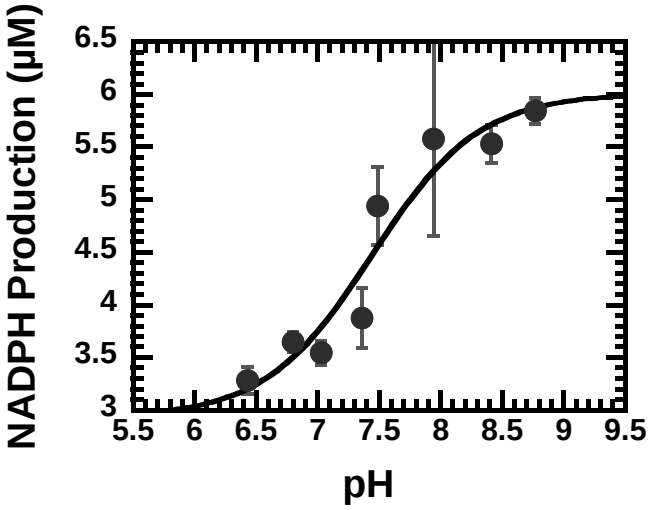

Fig. 7. pH-dependence of the NADPH production during the burst phase. Pre-steady state kinetics of NADPH production was monitored by absorbance increase at 340 nm using a stopped flow spectrophotometer at 4°C. A solution of 200 μM SSA and 300 μM $NADP^+$ was mixed against 10 μM *Ab*SSADHs. All concentrations are given as final concentrations. The pK_a value was calculated to be 7.4±0.2.

4.10 Reaction mechanism of *Ab*SSADH

The catalytic reaction of *Ab*SSADH is proposed as shown in Fig. 6. After the substrate binding (Step 1), the thiolate form of Cys289 first reacts with SSA to generate a thiohemiacetal intermediate (Step 2). A hydride equivalent is then transferred to $NADP^+$ to yield a thioester intermediate (Step 3). It is at this step that the absorbance

signal at 340 nm is generated because the pyridinium ring has acquired a hydride equivalent. The intermediate is expected to be hydrolyzed to generate the free enzyme and succinate. As a burst phase of absorbance at 340 nm could be detected, it indicated that the steps from substrate binding up to the hydride transfer to form NADPH (Steps 1-3) are faster than the following steps of thioester intermediate hydrolysis and product liberation (Steps 4-5). Therefore, the rate-limiting step of the overall reaction of *Ab*SSADH is at steps 4-5 of Fig. 6. Formation of Cys289 thiolate is necessary for the activity of *Ab*SSADH. Based on three independent methods of pK_a measurement, a p*K*a of Cys289 is 7.4-7.9.

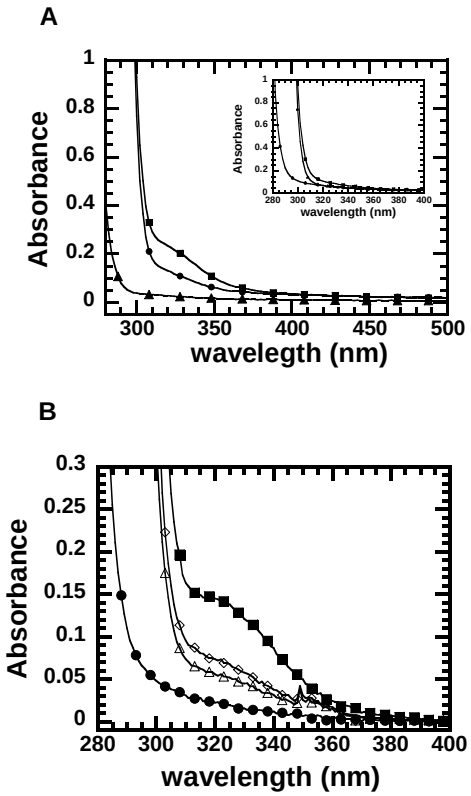

Fig. 8. Identification of NADP-cysteine adduct formation using spectrophotometry. (A) Spectra of 200 μM $NADP^+$ (circles), 200 μM *Ab*SSADH (triangles) and a mixture of 200 μM $NADP^+$ and 200 μM *Ab*SSADH (squares) after 2 h incubation at 25°C in 50 mM phosphate buffer pH 8 containing 1 mM DTT. Inset of (A) is spectra of 200 μM Cys289Ala incubated with 200 μM $NADP^+$ and 200 μM *Ab*SSADH or 200 μM $NADP^+$ alone. (B) Spectra of the NADP-cysteine adduct before (squares) and after separation by G-25 column. Spectra of eluted fractions containing protein are shown in empty diamonds and triangles.

5. Discussion

This report is the first to measure a pK_a value of the catalytic cysteine in *Ab*SSADH using transient kinetics, spectroscopic and pH-dependent studies. The methodology established based on burst kinetics and formation of NADP-cysteine adduct should be useful for studying the protonation state of active site cysteine in other ALDH enzymes in general. Investigation of catalytic properties of *Ab*SSADH also reveals that the enzyme has the highest catalytic turnover (k_{cat}) and lowest susceptibility to SSA substrate inhibition among all SSADHs known to date, suggesting that it has promising properties that make it advantageous for use in biotechnology applications. *Ab*SSADH is unique among all SSADHs in that the enzyme is located outside the GABA pathway and it prefers to use $NADP^+$ as a substrate while others SSADHs that are not part of the GABA degradation pathway do not have a preference towards $NADP^+$. Stopped-flow experiments detected burst kinetics at the first turnover of *Ab*SSADH, indicating that the hydride transfer to $NADP^+$ is faster than following steps.

The electron acceptor preference determination and sequence alignment analysis performed in this report have clearly shown that *Ab*SSADH is closely related to the GabD from the *gab* operon in *E. coli*. In bacteria, typically in *E. coli* and *S. typhimurium*, two SSADHs are present in their genome sequences [6, 7]. The first SSADH encoded by the *gabD* gene belongs to the *gab* operon [26]. The second SSADH is a gene product of the *yneI* gene that resides among the *yneJ*, *yneH* and *yneG* genes which code for a transcriptional regulator, glutaminase-2 and a putative protein with unknown function, respectively [27]. In the *A. baumannii* ZW85-1genome [26], three putative genes code for SSADH. One is located in the *gab* operon (AHB 89930.1) and contains the putative genes, *gabT*, *gabP* and *gabC* in the neighboring region. This gene arrangement is similar to the arrangement of the *gab* operon found in other bacteria [8]. The second (AHB91835.1) and third (AHB91335.1) putative SSADHs are located at a different genetic location. AHB91835.1 is located in a different genetic location from SSADH (YneI) identified in *E. coli* and *S. typhimurium* [6, 7]. The third SSADH (AHB91335.1) belongs to the operon involved in the 4-HPA degradation pathway which is similar to *Ab*SSADH reported here. Our results (Fig. 1 and 2) indicate that *Ab*SSADH from the 4-HPA degradation pathway has a protein sequence and substrate ($NADP^+$) preference similar to *E. coli* GabD rather than YneI.

Our results (Fig. 2) indicate that the enzyme prefers the use of $NADP^+$ as an electron acceptor over NAD^+ (10-fold higher in activity). YneI from *E. coli, Bacillus*

subtilis and *S. typhimurium* prefer to use NAD^+ over $NADP^+$ [6, 7, 9, 15]. The *E. coli* GabD can use both $NADP^+$ and NAD^+ as substrates, but exhibits much higher activity with $NADP^+$ (20-fold higher) than with NAD^+ [28]. Analysis of the cofactor and substrate selectivity in *Synechococcus* SSADH has suggested that residues at critical positions in the cofactor binding site are crucial for cofactor selectivity [21]. Polar residues with short side chains such as serine or threonine in the cofactor binding pocket prefer $NADP^+$ rather than NAD^+, while SSADHs with the negatively charged side chain of glutamate in the pocket prefer NAD^+ binding. SSADHs with other residues showed less differentiation in cofactor preference [21]. Based on the sequence alignment and the homology model (Fig. 2B and 2C), *Ab*SSADH contains Ser183 at the critical position of cofactor recognition, supporting the previously proposed explanation of the conserved Ser steering preference towards $NADP^+$ utilization.

Kinetic analysis of *Ab*SSADH revealed that the enzyme has a very high catalytic rate constant (k_{cat}= 137±9 s^{-1}) which is the highest among all SSADHs reported to date (Table 2). The k_{cat} values of most SSADHs are in the range of 5-10 s^{-1} [1, 14, 29, 30] except for the YneI ortholog from *S. typhimurium* which has a relatively high turnover number of 55 s^{-1} when used with NAD^+ as a hydride acceptor [7]. The k_{cat} value of *Ab*SSADH is 12-fold higher than that of SSADH from *Saccharomyces cerevisiae* at pH 8.4 (11 s^{-1}) [31]. *Ab*SSADH also displayed less SSA substrate inhibition compared to other SSADHs (Table 2). SSA concentrations had to be >500 μM to inhibit *Ab*SSADH activity, while potent SSA inhibition has been previously reported for SSADHs from various organisms including bacteria and fungi with inhibition observed at SSA concentrations >20 μM for SSADH from *S. pyogenes* and SSA >100 μM for SSADH from *S. typhimurium* [1, 7, 15, 19, 22, 32]. The crystal structure of a ternary complex of enzyme, substrate SSA and inhibitory SSA showed that the $NADP^+$ binding site can be bound by excess SSA, thus preventing the binding of $NADP^+$ [32]. Based on this information, we propose that the $NADP^+$ binding site in *Ab*SSADH has less preference for SSA binding compared to the $NADP^+$ binding site found in other enzymes. Unlike many of the other enzymes, *Ab*SSADH exhibited a high tolerance for succinic acid inhibition, retaining high activity in the presence of high succinic acid concentrations (up to 100 mM). We propose that in *Ab*SSADH, after succinic acid is formed, it can be rapidly and spontaneously released, causing no product inhibition [33]. In this regard, *Ab*SSADH is very attractive for biotechnological applications because it has a high catalytic turnover with low SSA (substrate) and succinic acid (product) inhibition as compared to the other SSADHs reported to date.

Table 2 Comparison of biochemical properties of *Ab*SSADH and SSADHs from other organisms.

Properties	Organisms						
	Bacteria					Yeast	Human
	***Ab*SSADH**[b]	***Ec*GabD**	***Mt*GabD**	***Sp*GabD**	***St*YneI**	***Sc*GabD**	***Hs*GabD**
Subunit mass (kDa)	52	52	54	52	49	54	61
Oligomer	tetramer	tetramer	ND	dimer	tetramer	tetramer	tetramer
$K_m^{app,SSA}$ (μM)[a]	189±31	8±1	3.0±0.2[c]	ND	27±5	15.5±0.1	2
$K_m^{app,\ NAD(P)+}$ (μM)	113±18	45±6	9±1[c]	100±10	43±3	579±30	40
k_{cat}^{app} (s^{-1})[a]	137±9	ND	4.7[c]	7.2±0.12	55±5	11.16	ND
SSA inhibition	>500 μM	ND	>20 μM	>20 μM	>100 μM	>100 μM	ND
K_i^{SSA} (μM)	ND	ND	(K_i^{app}= 62.8±12)	(K_i^{app}= 100±2)	ND	(K_i^{app}= 99.54)	ND
Ref.		[23,28]	[1]	[30,32]	[7]	[31]	[29]

Ec: *E. coli*, *Mt*: *M. tuberculosis*, *Sp*: *S. pyogenes*, *St*: *S. typhimurium*, *Sc*: *S. cerevisiae*, *Hs*: *H. sapiens* brain

ND =Not determined

[a] determined with preferred hydride acceptor

[b] two-substrate steady-state kinetics analysis

[c] in the presence of Mg^{2+} activator

*Ab*SSADH from the 4-HPA degradation pathway is a 2-cysteine SSADH (Cys289, Cys291) in which both active site cysteines are in the free thiol state in the active enzyme (Table 1). The ability of H_2O_2 to oxidize these two cysteines to give a di-sulfide linkage that is no longer reactive to Ellman's reagent (Table 1) implies that the free thiol groups of Cys289 and Cys291 in the active sites of the wild-type and variant *Ab*SSADHs are close to each other and accessible to outside solvent. This implies that with variation of redox status inside cells, the status of these active site cysteines can be modulated and this may be a means to control *Ab*SSADH activity. The disulfide formation between the two cysteines located in the catalytic loop has previously been found to cause a large structural change which resulted in inhibition of enzyme function in human GabD which contains Cys340 and Cys342 that are equivalent to Cys289 and Cys291 in *Ab*SSADH [12, 13, 15]. This redox-dependent regulation was proposed to be a way to regulate the physiological function of SSADH by sensing the change of environmental status [12]. For 1-cysteine SSADHs such as cyanobacterial SSADH, it was proposed that the adduct formation between the catalytic cysteine and $NADP^+$ may

act as a control mechanism by protecting the catalytic cysteine from H_2O_2 oxidation [14]. As the maximum activity of *Ab*SSADH was obtained when the enzyme was pretreated with DTT, we propose that the *Ab*SSADH activity can be regulated by cellular redox status.

The detection of burst kinetics of NADPH production by pre-steady state analysis indicates that the rate-limiting step of the *Ab*SSADH reaction occurs after the hydride transfer step (Fig. 4). This is the first detection of burst kinetics in the Class 5 ALDH family. Previously, burst kinetics was detected in the Class 1 and Class 2 ALDH enzymes such as human liver and sheep liver cytosol aldehyde dehydrogenases and nonphosphorylating glyceraldehyde-3-phosphate dehydrogenase from *Streptococcus mutans* [11, 34-37]. We propose that the rate-limiting step of the *Ab*SSADH reaction may be associated with the deacylation and product release steps. The mono-sigmoidal pH-rate profile of *Ab*SSADH k_{cat} showed a pK_a value of 7.5 (Fig. 5), suggesting that the overall rate-limiting step is associated with a deprotonated group with a pK_a of 7.5. This value is similar to the pK_a value of 7.5 of conserved Glu268, which plays a crucial role in the rate-limiting deacylation step reported in nonphosphorylating glycerldehyde-3-phosphate dehydrogenase from *S. mutans* [23, 38]. It is possible that the rate-limiting step of *Ab*SSADH reaction may be involved with the deacylation reaction.

The methodology established in this report directly probes the protonation state of Cys289. The techniques using magnitude of NADPH generated during the burst phase and formation of an NADP-cysteine adduct should be useful for investigating the cysteine protonation state of other enzymes in the ALDH superfamily in general. This method avoids interference from other cysteines in the protein. Other methods to probe cysteine ionization status such as the use of Ellman's reagent cannot be selective only to a catalytic cysteine. The pK_a value of catalytic Cys289 in *Ab*SSADH (7.5±0.1 measured from pH-rate profile, 7.4±0.2 from burst phase and 7.9±0.2 from the NADP-adduct formation) is ~0.6-1unit lower than the pK_a value of free Cys of 8.5 [39]. This may be a means of the *Ab*SSADH active site environment to enhance nucleophilicity of Cys289, because the thiolate form is more active nucleophile than the thiol form. Several factors have been reported to be important to increase catalytic cysteine reactivity in related aldehyde dehydrogenases [40, 41].

In conclusion, we have shown that *Ab*SSADH is a promising enzyme for biotechnology applications because it has the highest catalytic turnover (k_{cat}) and lowest susceptibility to SSA substrate inhibition among all SSADHs known to date. *Ab*SSADH is unique among all SSADHs in that the enzyme is located outside the GABA pathway

and it prefers to use $NADP^+$ as a substrate while others SSADHs that are not part of the GABA degradation pathway do not have a preference towards $NADP^+$. We also have established for the first time, the methodology to measure the catalytic cysteine pK_a in 2-cysteine SSADH using transient kinetics, spectroscopic and pH-dependent studies. This methodology should be useful for studying the protonation state of active site cysteine in other ALDH enzymes in general because the method is selective for measuring active site cysteine without interference from a neighboring cysteine.

5. References

1 De Caralho LPS, Ling Y, Shen C, Warren JD & Rhee KY (2011) On the chemical mechanism of succinic semialdehyde dehydrogenase (gabD1) from *Mycobacterium tuberculosis*. *Arch Biochem Biophys* **509**, 90-99.

2 Chambliss K L, Caudle DL, Hinson DD, Moomaw CR, Slaughter CA, Jakobs C & Gibson KM (1995) Molecular cloning of the mature NAD-dependent succinic semialdehyde dehydrogenase from rat and human cDNA isolation, evolutionary homology, and tissue expression. *J Biochem* **270**, 461-467.

3 Malaspina P, Roullet JB, Pearl PL, Ainslie GR, Vogel KR & Gibson KM (2016) Succinic semialdehyde dehydrogenase deficiency (SSADH): Pathophysiological complexity and multifactorial trait associations in a rare monogenic disorder of GABA metabolism. *Neurochem Int* **99**, 72–84.

4 Donnelly MI & Cooper RA (1981) Succinic semialdehyde dehydrogenase of *Escherichia coli:* their role in the degradation of *p*-hydroxyphenylacetate and γ-aminobutyrate. *Eur J Biochem* **113**, 555-561.

5 Thotsaporn K, Tinikul R, Maenpuen S, Phonbuppha J, Watthaisong P, Chenprakhon P & Chaiyen P (2016). Enzymes in the *p*-hydroxyphenylacetate degradation pathway of *Acinetobacter baumannii*. *J Mol Catal B: Enzym* **134**, 353–366.

6 Fuhrer T, Chen L, Sauer U & Vitkup D (2007) Computational prediction and experimental verification of the gene encoding the NAD^+/$NADP^+$-dependent succinate semialdehyde dehydrogenase in *Escherichia coli. J Bacteriol* **189**, 8073-8078.

7 Zheng H, Beliavsky A, Tchigvintsev A, Brunzelle JS, Brown G, Flick R, Evdokimova E, Wawrzak Z, Mahadevan R, Anderson WF, Savchenko A & Yakunin AF (2013) Structure and activity of the $NAD(P)^+$-dependent succinic

semialdehyde dehydrogenase YneI from *Salmonella typhimurium*. *Proteins* **81**, 1031-1041.

8 Bartsch K, Marteville AVJ & Schulz A (1990) Molecular analysis of two genes of the *Escherichia coli gab cluster*: Nucleotide sequence of the glutamate: succinic semialdehyde transminase gene (gabT) and characterization of the succinic semialdehyde dehydrogenase gene (gabD). *J Bacteriol* **172**, 7035-7042.

9 Marek LE & Henson JM (1988) Cloning and expression of the *Escherichia coli* K-12 sad gene. *J Bacteriol* **170**, 991-994.

10 Prieto MA, Diaz E & García JL (1996) Molecular characterization of the 4-hydroxyphenylacetate catabolic pathway of *Escherichia coli* W: engineering a mobile aromatic degradative cluster. *J Bacteriol* **178**, 111-120.

11 Marchal S, Rahuel-Clermont S, & Branlant G (2000) Role of glutamate-268 in the catalytic mechanism of nonphosphorylating glyceraldehyde-3-phosphate dehydrogenase from *Streptococcus mutans*. *Biochemistry* **39**, 3327-3335.

12 Kim YG, Lee S, Know OS, Park SY, Lee SJ, Park BJ & Kim KJ (2009) Redox-switch modulation of human SSADH by dynamic catalytic loop. *EMBO J* **28**, 959-968.

13 Langendorf CG, Key TLG, Fenalti G, Kan WT, Buckle AM, Davies TC, Tuck KL, Law RHP & Whisstock JC (2010) The X-ray crystal structure of *Escherichia coli* succinic semialdehyde dehydrogenase; structural insights into $NADP^+$/enzyme interactions. *PLoS One* **5**, e9280.

14 Park J & Rhee S (2013) Structural basis for a cofactor-dependent oxidation protection and catalysis of *cyanobacterial* succinic semialdehyde dehydrogenase. *J BiolChem* **288**, 15760-15770.

15 Ahn JW, Kim YG & Kim KJ (2010) Crystal structure of non-redox regulated from *Escherichia coli. Biochem Biophys Res Commun* **392**, 106-111.

16 Muñoz-Clares RA, González-Segura L, Riveros-Rosas H & Julián-Sánchez A (2015) Amino acid residues that affect the basicity of the catalytic glutamate of the hydrolytic aldehyde dehydrogenases. *Chem Biol Interact* **234**, 45-58.

17 Jackson B, Brocker C, Thompson DC, Black W, Vasiliou K, Nebert DW & Vasiliou V (2011) Update on the aldehyde dehydrogenase gene (ALDH) superfamily. *Human genomics* **5**, 283-303.

18 Díaz E, Ferrández A, Prieto MA & García JL (2001) Biodegradation of aromatic compounds by *Escherichia coli*. *Microbiol Mol Biol Rev* **65**, 523-569.

19 Kumar S, Kumar S & Punekar NS (2015) Characterization of succinic semialdehyde dehydrogenase from *Aspergillus niger*. *Indian J ExpBiol* **53**, 67-74.

20 Narayan VS & Nair PM (1989) Potato Tuber succinate semialdehyde dehydrogenase: purification and characterization. *Arch Biochem Biophys* **275**, 469-477.

21 Yuan Z, Yin B, Wei D & Yuan YRA (2013) Structural basis for cofactor and substrate selection by cyanobacterium succinic semialdehyde dehydrogenase. *J Struct Biol* **182**, 125-135.

22 Rivett AJ & Tipton KF (1981) Kinetic studies with Rat-Brain succinic semialdehyde dehydrogenase. *Eur J Biochem***117**, 187-193

23 Cozzani I, Fazio AM, Felici E & Barletta G (1980) Separation and characterization of NAD- and NADP-specific succinate-semialdehyde dehydrogenase from *Escherichia coli* K-12 3300. *Biochim BiophysActa* **613**, 309-317.

24 Marchal S & Branlant G (1999) Evidence for the chemical activation of essential cys-302 upon cofactor binding to nonphosphorylating glyceraldehyde 3-phosphate dehydrogenase from *Streptococcus mutans*. *Biochemistry* **38**, 12950-12958.

25 Wymore T, Deerfield DW & Hempel J (2007) Mechanistic implications of the cysteine-nicotinamide adduct in aldehyde dehydrogenase based on quantum mechanical/molecular mechanical simulations. *Biochemistry* **46,** 9495–9506.

26 Wang X, Zhang Z, Hao Q, Wu J, Xiao J & Jinga H (2014) Complete genome sequence of *Acinetobacter baumannii* ZW85-1. *Genome A.***2**, e01083-13.

27 Riley M, Abe T, Arnaud MB, Berlyn MK, Blattner FR, Chaudhuri RR, Glasner JD, Horiuchi T, Keseler IM, Kosuge T, Mori H, Perna NT, Plunkett G, Rudd KE, Serres MH, Thomas GH, Thomson NR, Wishart D & Wanner BL (2006) *Escherichia coli* K-12: a cooperatively developed annotation snapshot--2005. *Nucleic Acids Res* **34**, 1-9.

28 Jaeger M, Rothacker B & Ilg T (2008) Saturation transfer difference NMR studies on substrates and inhibitors of succinic semialdehyde dehydrogenase. *Biochem Biophys Res Commun* **372**, 400-406.

29 Park SA, Park YS & Lee KS (2014) Kinetic characterization and molecular modeling of NAD (P)$^{+}$-dependent succinic semialdehyde dehydrogenase from *Bacillus subtilis* as an ortholog YneI. *J Microbiol Biotechnol* **24**, 954-958.

30 Jang EH, Park SA, Chi YM & Lee KS (2014) Kinetic and structural characterization for cofactor preference of succinic semialdehyde dehydrogenase from *Streptococcus pyogenes*. *Mol Cells* **37**, 19-26.

31 Cao J, Singh NK & Locy RD (2014) Characterization of the recombinant succinic semi-aldehyde dehydrogenase from *Saccharomyces cerevisiae*. *Yeast* **31**, 411-420.

32 Jang EH, Park SA, Chi YM & Lee KS (2015) Structural insight into the substrate inhibition mechanism of NAD^+-dependent succinic semialdehyde dehydrogenase from *Streptococcus pyogenes. Biochem Biophys Res Commun. **461**, 487-93*.

33 Cornish-Bowden A (2012). *Fundamentals of enzyme kinetics*, 4th Ed., Wiley-VCH Verlag & Co. Weinheim, Germany

34 Vallari RC & Pietruszko R (1981) Kinetic mechanism of the human cytoplasmic aldehyde dehydrogenase E1. *Arch Biochem Biophys* **212**, 9-19.

35 Ambroziak W, Kosley LL & Pietruszko R (1989) Human aldehyde dehydrogenase: coenzyme binding studies. *Biochemistry* **28**, 5367-5373.

36 Farres J, Wang X, Takahashis K, Cunningham SJ, Wangn TT & Weiner H (1994) Effects of changing glutamate 487 to lysine in rat and human liver mitochondrial aldehyde dehydrogenase. *J Biol Chem* **269,** 13854-13860.

37 Farres J, Wang TT, Cunningham SJ & Weiner H (1995) Investigation of the active site cysteine residue of rat liver mitochondrial aldehyde dehydrogenase by site-directed mutagenesis. *Biochemistry* **34**, 2592-2598.

38 Marchal S, Rahuel-Clermont S & Branlant G (2000) Role of glutamate-268 in the catalytic mechanism of nonphosphorylating glyceraldehyde-3-phosphate dehydrogenase from *Streptococcus mutans*. *Biochemistr*y **39**, 3327-3335.

39 Lim CJ, Gruschus JM, Kim G, Berlett BS, Tjandra N & Levine RL (2012) A low pK_a cysteine at the active site of mouse methionine sulfoxide reductase A. *J Biol Chem*. **287,** 25596–25601.

40 Wang X & Weiner H (1995) Involvement of glutamate 268 in the active site of human liver mitochondrial (Class 2) aldehyde dehydrogenase as probed by site-directed mutagenesis. *Biochemistry* **34**, 237–243.

41. Marchal S & Branlant G (1999) Evidence for the chemical activation of essential cys-302 upon cofactor binding to nonphosphorylating glyceraldehyde 3-phosphate dehydrogenase from *Streptococcus mutans.* Biochemistry **38**, 12950-12958.

42. Thotsaporn K, Sucharitakul J, Wongratana J, Suadee C & Chaiyen P (2004) Cloning and expression of *p*-hydroxyphenylacetate 3-hydroxylase from *Acinetobacter baumannii:* evidence of the divergence of enzymes in the class of two-protein component aromatic hydroxylases. *Biochim Biophys Acta* **1680**, 60-66.

43 Riener CK, Kada G & Gruber HJ (2002) Quick measurement of protein sulfhydryls with Ellman's reagent and with 4,4′-dithiodipyridine. *Anal Bioanal Chem* 373:266–276.

44. Chenprakhon P, Trisrivirat D, Thotsaporn K, Sucharitakul J & Chaiyen P (2014) Control of C4a-hydroperoxyflavin protonation in the oxygenase component of p-hydroxyphenylacetate-3-hydroxylase. *Biochemistry* ***53***, 4084-4086.

45. Pinthong C, Maenpuen S, Amornwatcharapong W, Yuthavong Y, Leartsakulpanich U & Chaiyen P (2014) Distinct biochemical properties of human serine hydroxymethyltransferase compared with the Plasmodium enzyme: implications for selective inhibition. *FEBS J* ***281***, 2570-2583.

46. Arnold K, Bordoli L, Kopp J & Schwede T (2006) The SWISS-MODEL Workspace: A web-based environment for protein structure homology modelling. *Bioinformatics* **22,** 195-201.